

In Situ and Time Resolved Carbonaceous Matter Oxidation Studies with Indirect Nanoplasmonic Sensing

FARZIN JAHANGIRI

Department of Applied Physics
Competence Center for Catalysis
CHALMERS UNIVERSITY OF TECHNOLOGY
Göteborg, Sweden 2013

MASTER'S THESIS 2013

In Situ and Time Resolved Carbonaceous Matter Oxidation Studies
with Indirect Nanoplasmonic Sensing

FARZIN JAHANGIRI



CHALMERS

Department of Applied Physics
Division of Chemical Physics
Competence Center for Catalysis (KCK)
CHALMERS UNIVERSITY OF TECHNOLOGY
Gteborg, Sweden 2013

In-Situ and Time Resolved Carbonaceous Matter Oxidation Studies with Indirect Nanoplasmonic Sensing

© FARZIN JAHANGIRI, 2013

Examensarbete / Institutionen för Teknisk Fysik,
Chalmers Tekniska Högskola

Department of Applied Physics
Division of Competence Center for Catalysis (KCK)
Chalmers University of Technology
SE-412 96 Göteborg
Sweden
Telephone: + 46 (0)31-772 1000

Cover:

Typical source and morphology of the diesel exhaust particulate (left), INPS platform and sensing apparatus (middle) and curves representing the oxidation behaviour of graphitic carbon material used in this study obtained with INPS (right).

Printed at Chalmers Reproservice
Göteborg, Sweden 2013

In-Situ and Time Resolved Carbonaceous Matter Oxidation Studies with Indirect Nanoplasmonic Sensing

Master of Science Thesis in the Masters Programme Applied Physics

FARZIN JAHANGIRI

Department of Applied Physics

Competence Center for Catalysis (KCK)

Chalmers University of Technology

ABSTRACT

This work aims at assessing the oxidation of carbonaceous matter with a novel optical experimental technique named Indirect Nanoplasmonic sensing (INPS). The INPS working principle is based on the optical absorption profile of metallic nanoparticles via the excitation of localized surface plasmon resonances and was, in this work, utilized for the first time to monitor in situ and in real time un-catalyzed O_2 -based oxidation of nanoscopic carbon materials.

Oxidation of carbon-based materials is central in a wide range of industrial applications as well as in energy production based on fossil fuels, and in environmental cleanup processes. In particular, under the category of transport emission reduction in the process of regenerating Diesel Particulate Filters (DPF), understanding the oxidation reaction of carbonaceous matter known as soot is of high importance in order to meet more and more stringent emission legislations, which are imposed due to the health risks associated with soot nanoparticles. Two types of carbonaceous matter were used in this study, Printex U commonly used as a model for diesel soot and graphitized carbon films in the main part of the project. The Printex U study, due to the problems mainly associated with deposition on INPS sensor chips, turned out to require efforts beyond the scope of this work to derive an optimal deposition protocol and is thus only discussed in the appendix. INPS showed in general a high sensitivity towards oxidation rates of graphitic carbon films as a function of temperature and oxidant concentration. From progressive isothermal oxidation experiments, relevant kinetic parameters could be extracted, such as an activation energy of around 135 kJ/mol. Differential and pulsed oxidation experiments were used to extract the reaction order, which was found to be 1 for oxygen. Both these values are in agreement with the range of reported values in the literature. In connection to the reactivity of carbon films, conversion dependencies were assessed and found to agree well with previous published results. Finally, also the oxidation history of the carbon films, that is to what oxidation conditions the films have been exposed previously, was shown to be important as it modifies the rate of the further oxidation. Due to the complexity of the carbon oxidation process (e.g. sites with different reactivities, time-dependent number of active sites, etc.), and due to issues originating arguably from the chosen deposition procedure of the carbon films (i.e. thermal evaporation), a high degree of reproducibility for the progressive isothermal oxidation experiments could not be achieved. In connection to the INPS platform, due to the fact that sensitivity of plasmonic signal is a function of several parameters such as temperature, distance of the reaction from the sensor surface and more, the comparison of the different temperature results and different film thicknesses are subject to limitations. Possible improvements to eliminate/minimize such effects are thus also discussed.

Keywords:

Carbon oxidation, Nanoplasmonic sensing, INPS, *In-situ*, real time, Soot oxidation, kinetic analysis, un-catalyzed oxidation, emission cleaning, diesel particulate filter, regeneration

Contents

1	Understanding Soot Oxidation with Nanoplasmonics	1
1.1	Background	1
1.2	Objective	2
2	Introductory Concepts	3
2.1	Carbonaceous Matter: Characteristics and Oxidation	3
2.1.1	Formation	3
2.1.2	Structure	3
2.1.3	Surface Area	5
2.1.4	Mechanism	7
2.1.5	Oxidation Kinetics	8
2.1.6	Model carbon	9
2.2	Nanoplasmonics: The Physics and Technology	9
2.3	References	11
3	Materials and Methodology	13
3.1	INPS Sensor chips	13
3.2	Deposition and Calibration of Model Soot	13
3.2.1	Physical shaking method of Printex U model soot	14
3.2.2	Other Methods For Deposition of Printex U soot on INPS sensor chips	14
3.3	Carbon film deposition	14
3.4	Measurement Signals	14
3.5	Carbonaceous Matter Oxidation Studies with INPS	15
3.5.1	Printex U Step Response Oxidation	15
3.5.2	Step-Response oxidation of Graphitized Carbon	15
3.5.3	SEM Imaging of the carbon films	15
3.5.4	Sweep Experiments	16
3.5.5	Conversion Dependence of the Reaction Rate	17
4	Results and Discussions	18
4.1	Isothermal Oxygen Step-Response Experiments	18
4.1.1	5 nm thick films	18
4.1.2	10 nm thick films	18
4.1.3	Double channel oxidation	21
4.1.4	Activation energy estimation in the Arrhenius coordinates	24
4.2	Oxygen Sweep Experiments	28
4.2.1	Oxygen reaction order	28
4.2.2	Carbon film qualitative investigations with Oxygen Sweep	30
4.3	References	36

5	Concluding Remarks	37
6	Outlook	39
7	Acknowledgement	41
8	Appendix A: Printex U model Soot deposition and Oxidation Studies with INPS	43

Chapter 1

Understanding Soot Oxidation with Nanoplasmonics

1.1 Background

Soot is formed under non-stoichiometric combustion of hydrocarbon-based fuels such as wood, coal and fossil fuels, i.e. gasoline and diesel. For this reason soot is also a common constituent in automotive particulate matter (PM) emissions. Soot is one of the most problematic carbonaceous materials for the environment and health. In the atmosphere, micro- to nano-scale soot particles can cause a warming effect up to 60% that of carbon dioxide (1). Concerning health effects, recent studies show that PM is more detrimental to the human respiratory system (2) than previously thought both for long- and short-term exposure to fine PM_{2.5} (size fraction below 2.5 μm) and ultrafine PM_{0.1} (size fraction below 0.1 μm) particles. Thus it is important to target low formation of PM and soot emissions as also ever stringent legislations in most of the industrialized countries are in effect (3). Within the automotive sector additional exhaust aftertreatment technologies, i.e. catalytic soot filters capable of oxidizing soot into carbon dioxide and water, are often included in the exhaust pipe downstream the engine. The present aftertreatment technologies, however, need to be improved further to target future low emission levels of PM as imposed by legislation.

From an academic point of view, to form a knowledge-based development of catalytic soot filters, it is important to unravel the underlying mechanisms behind catalytic soot oxidation. The open scientific literature concerning soot oxidation offers an extensive pool of studies with different methods, usually ex situ techniques. For an overview of methods and estimation of kinetic parameters, see for example Refs. (4) & (5). These studies have brought quite some light into the subject. There are, however, a number of inherent complicating factors in many studies that may lead to contradictory results. Among these one finds: i) lack of experimental techniques for time-resolved studies of the oxidation reactions in situ, resulting in, e.g., poor agreement between reported kinetic parameters, ii) lack of theoretical models that can fully explain the complexities associated with empirical data and finally iii) rather large variations in the nature and composition of diesel soot at different locations and various local conditions of its formation such as fuel type and engine operation mode and particulars.

To fully understand the governing mechanisms and considering the effect of all ambient parameters on soot oxidation it is crucial to seek for new opportunities that can provide new windows into the reaction under realistic exhaust conditions i. e. in situ and in real time. Recent trends in physical chemistry and catalytic studies have grown hectic to incorporate the optical properties of noble metal nanoparticles - called Localized Surface Plasmon Resonance (LSPR) - as probe to magnify the ongoing reaction schemes happening in a close enough proximity and in a diverse range of applications such as bio- and chemical sensors. In this regard, a newly developed optical method at Chalmers called Indirect Nanoplasmonic Sensing (INPS) (6) has been proposed for soot oxidation studies. This method is working on the principle of sensing and tracking the plasmonic excitations of gold nanoparticles nanofabricated on the state of the art sensor chip. It is best

suites to study the changes and processes of the target materials adjacent to sensor nanoparticles, which will be solid carbonaceous matter in this thesis. Since INPS is an optical technique it provides the possibility to remotely read off the signal from the reactive environment at high temperatures and under precise conditions. Among other features of INPS lies the versatility of this nano-optical probe, which can be adjusted to work in many different ambient and contact conditions with a wide range of target material. INPS offers very high sensitivity to the changes originating from reaction and use a different mechanism to look into the reaction by providing temporal resolutions of readouts in the millisecond range. Additionally, INPS has proven to be quite successful in other studies measuring tiny changes of optically sensitive phenomena such as hydrogen storage (7) optical calorimetry, catalysis and glass transitions (8) motivating its beneficial incorporation in this study. Utilization of INPS would seem to bring new possibilities and dimensions of information about the soot oxidation studies.

1.2 Objective

The objective with the present work is to demonstrate, for the first time, how INPS can be used for in situ studies of soot oxidation. By performing kinetic oxidation experiments with Printex U, a carbon black material commonly considered to mimic diesel soot well, and graphitized carbon at different temperatures and oxygen concentrations, global kinetic information, i.e. Arrhenius parameters, is extracted and compared with corresponding values reported in the open literature. The applicability of the INPS method as well as some guidelines for future studies are discussed.

Chapter 2

Introductory Concepts

2.1 Carbonaceous Matter: Characteristics and Oxidation

2.1.1 Formation

Fraction of the diesel particulate matter known 60 % as soot is formed from the nucleation of uncharged radicals and molecules within the exhaust flames during combustion at high temperatures as result of poor mixing of oxygen and fuel at the molecular level. The nucleation units grow continuously as the flame cools down. The presence of other gaseous hydrocarbons such as C_2H_2 , C_2H_4 , polycyclic aromatic hydrocarbons (PAH) (1) and also double and triple bonded (unsaturated) carbon species (2) in a repetitive growth process give rise to hierarchical structures. One of the main pathways leading to such structures is depicted in Figure 1. The first and finest species to form are called spherules with diameters in the range of 10-50 nm. These spherules in turn, coagulate to particles within the range of 0.1-1 μm due to the shared adsorbates. The particles subsequently also tend to form agglomerates in the size range of 1-100 m. Such structuring is a result of surface forces, which can be influenced by adsorbed species on the carbonaceous particle surface, such as ash or soluble organic fraction SOF (determined by chemical extraction Soxlet method) from fuel and lubricating oil, inorganic compounds (mostly sulphates originating from fuel) and water. Moreover, a small fraction of the produced soot is ash, whose content can vary significantly depending on the fuel and engine type, driving mode, additives and engine metallurgical materials, includes phosphates and various metal oxides. In summary, it becomes clear the soot from a diesel engine is a very heterogeneous material, both in terms of chemical composition and the sizes of the constituent particles.

Studies of typical diesel soot have shown the elemental composition ranges on a mass basis enlisted in table 1 (3).

Typical Soot Composition	C	H	N	O	S
Element wt(%)	69-90	1-4	<1.2	4-13	0.05-1.1

Table 1- Typical Soot analysis

2.1.2 Structure

Soot structure at its smallest scale, as revealed in X-ray and electron microscopy studies, exhibits graphitic crystallite units with diameter of 1.2nm (4), which are turbostratically packed (having graphene layers displaced compared to each other in graphitic structure) with an interlayer spacing of 0,35 nm, i.e. slightly larger than in pure graphite. Also the crystallites are situated in a concentric manner giving form to an onion like shell with increased disorder toward the core of the particle, as illustrated in figure 2-(a) (5) and as aggregated in larger clusters in figure 2-(b) (2).

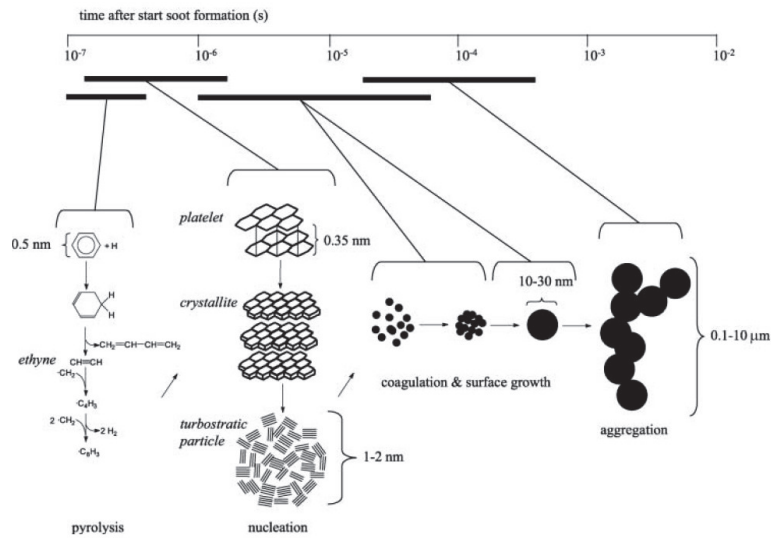


Figure 1- Formation stages of Soot agglomerates. Firstly, certain species are pyrolyzed into unsaturated molecules mostly ethyne and then ethyne polymerizes into polyethyne. When such chains come across they form the poly ring structure unites which are called platelets. Platelets are stacked to form crystallites, which in turn pack together to form Turbostratic particles as nucleation unites. These particles undergo surface growth and coagulation to form primary soot particles and even by further agglomeration they form the chain like aggregates.

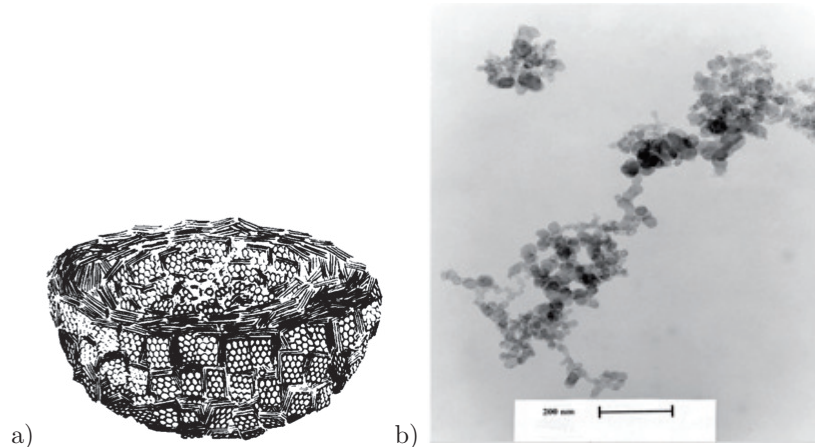


Figure 2 (a) Detailed model of the spherule structure proposed from lattice fringe imaging technique, which provides details on more structured part of carbon. (b) The agglomerates of soot imaged in TEM microscope, showing clumps of spherules.

As it is well-known for the soot to have a wide range of structural and chemical property variations, which sensitively depend on the fuel nature, engine design, exhaust condition and sampling technique, and consequentially different kinetics and reaction responses, certain studies have been conducted to explain these data, such as reaction rate dependency on the account of initial carbon nanostructures. For instance, Vander Wal et. al. (6) has investigated the influence of length and curvature of graphitic shell grains (from different synthesis methods and fuel types) on the oxidation rate using High Resolution TEM nanography shown in figure 3. In addition, porosity, crystallinity and size distribution of the carbonaceous particulate matter are among physical properties which influence the kinetics of the oxidation reaction.

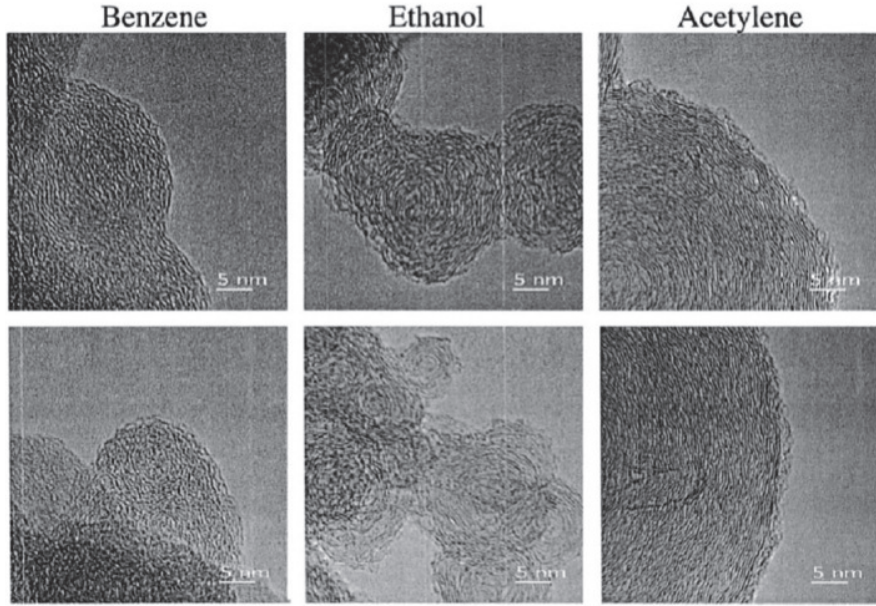


Figure 3- Soot nanostructures as a result of different fuels and pyrolysis conditions. Grain curvature and texture for different soots derived from pyrolysis of three differe substances. Images acquired by HRTEM.

2.1.3 Surface Area

The total surface area (TSA) of soot varies in a range of 20-230 m^2/gr measured by BET analysis and nitrogen as adsorbate (2). For particles with 25nm diameter and density of 2000 kg/m^3 the theoretical surface area is 120 m^2/gr so the pore surface is not significantly large. Studies show an increased specific surface area of 270 m^2/gr when the material is heated to 600° C under inert atmosphere which indicates that SOF content tend to block some present micropores in the material. Total number of carbon active sites N_T is dependent on the actual surface area and the concentration of the active sites (7):

$$N_T = \lambda \frac{S}{S_0}$$

Where λ is concentration of active sites, S the actual surface area and S_0 is the initial surface area. There are several studies to account for pore surface area (S) geometry and growth versus conversion such as the random pore model and simpler nth-order model which is briefly mentioned here:

$$\frac{S}{S_0} = (1 - \zeta)^{n_\zeta}$$

Where ζ is the conversion degree and n_ζ is the reaction order with carbon. In the case of $n_\zeta = 2/3$ the nth-order model is called shrinking core model. This model however is not very accurate since in highly porous carbon such as real soot and activated carbon the pores form a complex network. With progressive oxidation, growing new pores and opening of blocked pores, the surface area increases and could results in ramped up oxidation rate. To further illustrate this, other studies such as one by Bhatia and Perlmutter proposed geometrical overlapping pore surfaces such as cylindrical and spheres figure 4(a) and pore network topology figure 4(b) with three coordinates (8) & (9).

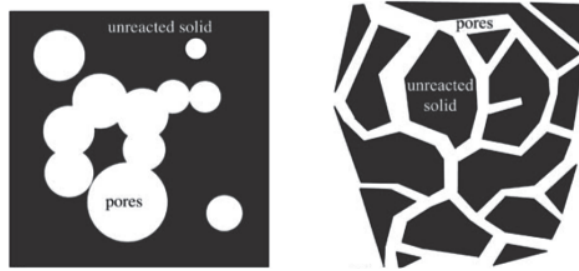


Figure 4-Different models describing the conversion. (a) The cylindrical surface description of pore and (b) the three-coordinated Bethe network (adopted from (8) & (9))

Active Surface Area (ASA), the fraction of the total surface area that is chemically active during gasification of carbon, is referred to the sites predominantly contributing to the rate which include the defect centers in basal planes, edge plains of the graphitic planes, prismatic and pyramidal faces shown in figure 4. This is due to the fact that the activation barrier on such sites is lower as compared to the basal and perfect planes (10) due to the higher surface energies at the defects and edge planes (11).

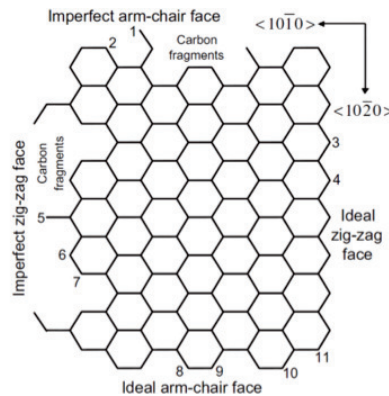


Figure 5- Edge plane sites of the graphitic sheet.

In connection to the TSA and graphitic microstructure changes with conversion, a direct relationship between total surface area (TSA) and ASA hasnt been found (10). For different types of the carbon the active surface area versus conversion is plotted in figure 6.

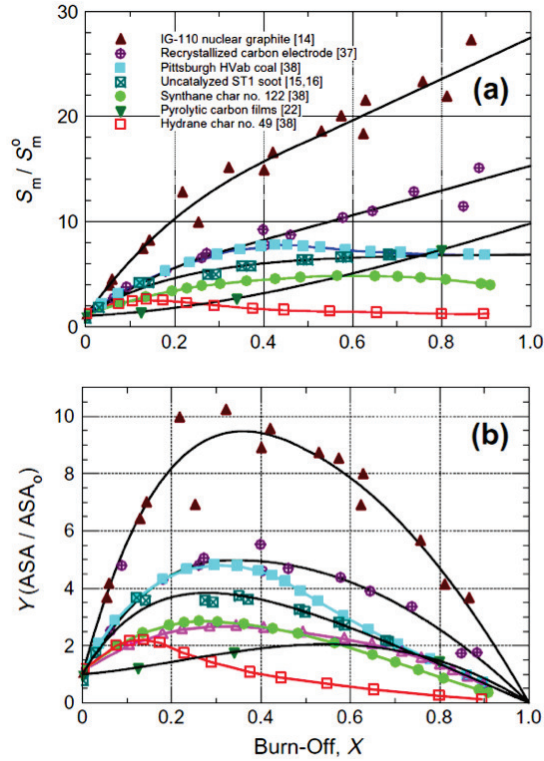


Figure 6- Active surface area for different types of carbon material and the dependency on the burn-off: (a) normalized specific ASA, (b) normalized ASA, adopted from (10).

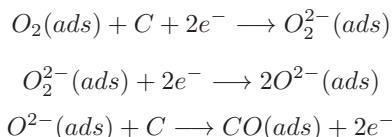
Pore volume initially starts to grow throughout the bulk material and reaches a maximum as conversion proceeds. As it continues, the pore start to meet and merge into each other, causing a reduction in total surface area.

In an investigation of annealing effects on sputtered carbon films by SEM it was revealed that the ordering of the crystallites increases as a result of an increasing fraction of SP2 bonding and ordering of SP2 clusters in the carbon network (12) which, in principle counteracts the abundance of active and high energy sites prone to oxidation initiation. This ordering has also been observed in annealed carbon nanoparticles by SEM studies in another work (unpublished) at Chemical Physics division, Chalmers.

2.1.4 Mechanism

The oxidation of carbonaceous matter can occur with various oxidants such as O_2 , O , CO_2 , NO , NO_2 , H_2O and OH radicals. In this study O_2 -based oxidation processes will be considered. The oxidation requires oxygen to reach and adsorb on to the carbon surface, and the formation of surface oxide complexes, rearrangement and desorption of the products. In the literature there is an abundance of reports on reaction steps, species involved and activation energies for different carbon types and products. They are reviewed comprehensively for example in (2). Nevertheless, the following scenarios are generally accepted to hold for oxygen as oxidant on graphitic surfaces: The reaction mechanism of an oxygen molecule with the carbon surface has been proposed by two distinct models, i) direct collision of the O_2 molecule with the reactive sites of the carbon surface following an Eley-Rideal (ER) mechanism; ii) physisorption of O_2 molecules on the non-reactive basal surface of carbon, migration on the surface and reduction upon reaching the reactive sites by the Langmuir-Hinshelwood (LH) mechanism. For the reaction to happen the oxygen must be activated by undergoing charge transfer with the carbon and turning into oxide ions such superoxide (O_2^-) and peroxide

(O_2^{-2}). When oxygen is on the basal planes of the graphitic surface as a physisorbed molecule the charge transfer is prevented due to a kinetic barrier. As it reaches to the defect sites and edge planes, it can undergo reduction to form the mentioned oxide species, which then is able to form stable covalent bonds with carbon atoms:



For the direct collisions of molecular oxygen on the defect sites i.e. reactive sites, the O-O bond, as a result of the repulsive intermolecular forces undergoes an exothermic breaking without any activation energy and finally forms the carbon-oxygen functional groups.

2.1.5 Oxidation Kinetics

To gain insight into the reaction scheme of carbonaceous matter oxidation, kinetic studies provide a basis to bridge macroscopic events and parameters, and molecular level processes. Moreover, such studies importantly used to investigate the connection between crucial features of reaction such as rate and reactivity to the physical and chemical conditions subject to the reacting species. There is a number of global kinetic models used in the literature, the most common of which in carbonaceous oxidation with O_2 is the global rate law of Arrhenius:

$$\begin{aligned} r &= K(T)N_tP_{O_x}^{n_{O_x}} \\ K(T) &= Ae^{-E_a/(RT)} \\ N_t &= m_{C,initial}(1-x)^{n_C} \end{aligned}$$

where r represents the reaction rate, $K(T)$ is the Arrhenius rate constant with A pre-exponential factor, E_a the activation energy, R the gas constant, T the absolute temperature, $P_{(O_x)}$ and $n_{(O_x)}$ are partial pressure and reaction order of oxygen respectively. N_t represents the number of active sites, which is determined by the chemically active portion of the total surface area and is a function of the conversion. Therefore, at each conversion degree, the reaction rate must be normalized by a function representing the ASA. Here the simple n th order model is used to derive such a function, where $m_{(C,initial)}$ is the carbon amount at the start of the experiment, x the mole fraction of the converted carbon, and n_C is the reaction order of the carbon. Even though this model doesn't fully explain the evolution of the ASA with conversion, compared to other suggested models and due to its simplicity it is mostly used and experimental data are used to find the best fit for it. For example the model predicts a decrease in the ASA with conversion whereas the reaction rate increases initially with conversion. It could be indicative of other ongoing processes such as pore volume growth and opening of occluded ones which need to be considered and few models are suggested to describe such growth (mentioned above (8) & (9)). Ultimately, the normalized reaction rate by an actual ASA, in principle, must reflect a constant value, which is required to report conversion-independent kinetic parameters given the homogeneity of carbon and out of limiting regimes.

The sought-after kinetic parameters would be $n_{(O_2)}$, n_C , E_a and A and in order to determine them as a complete set, a series of oxidation data within a range of temperatures and partial oxygen pressures needs to be collected. Oxidative experiments can be performed in a step-response (SR) or a temperature programmed oxidation (TPO) fashion or both as complementary methods. In this work, isothermal oxidations are performed and a linearized version of the rate equation is solved to analyze the obtained results.

2.1.6 Model carbon

Due to variations in chemical composition and physical properties of carbonaceous particulate matter stemming from a number of factors such as fuel type, exhaust condition, sample collection method and etc. it is difficult to draw consistent conclusions about soot oxidation behavior in terms of mechanism and global kinetics. Thus it is inevitable to turn to more homogenous synthetic materials as model for scientific studies and systematic tracking of influencing parameters. Different commercial model carbons are currently used with very similar properties to diesel soot. The first use of model carbon in relation to automotive PM reduction studies was introduced by Neeft at Delft University at 1992, and since then has become the major working material for many other groups. In this work Printex-U and mostly graphitic carbon powder are incorporated in studies.

2.2 Nanoplasmonics: The Physics and Technology

Interaction of light with geometrically nanoconfined metallic material such as thin films and nanoparticles of metals like gold and silver, thanks to their internal electronic structure, forms the backbone of the optical nanoscopy technique being used in this work. Entrapment or coupling of light radiation with surface waves of metal free electrons give rise to so-called surface plasmons (SP). These plasmon waves are strongly bound to surface, in this context, the metal and dielectric interface. Depending on the dimensionality of the material, SPs can either propagate at an extended metal film interface or become localized in a nanoparticle (13). The latter gives rise to localized surface plasmon resonance (LSPR) which is utilized in the Indirect Nanoplasmonic Sensing (INPS) technology (14) for sensing application broadly towards material science (15). The working principle of INPS involves collective and coherent oscillations of conduction band electrons of the metallic nano-disks upon exposure to the electromagnetic radiation at the surface boundary of metal/dielectric. In the particle size range of sub-wavelength (100 nm), the electron oscillation is considered to be spatially uniform throughout the particle and corresponds to a dipolar standing wave mode of charge density against the positive ionic lattice (LSPR). The resonance frequency of this plasmonic excitation is sensitively a function of several parameters including size and geometry of the particle, temperature, material and environment of the metallic nanoparticles. The resonance frequency of the nanoparticle LSPR can be estimated by the following relation (16):

$$\omega_p = \sqrt{\frac{Ne^2}{3m_e\epsilon_0}}$$

With N being the electron density, e the electron charge, m_e the effective electron mass and ϵ_0 the vacuum permittivity. As a result of local charge separation during LSP oscillation, LSP causes field enhancement extending perpendicularly out from the surface and decaying exponentially with distance, penetrating through and over the thin dielectric layer which is covering the nano-disks. Such field enhancement is of evanescent nature (13). Since LSPR of gold particles is highly sensitive to its environment, occurring physical or chemical process such the progressive carbon oxidation reaction under study in this project, induces changes in optical properties (refractive index) of the dielectric layer covering the gold nano-sensors. This, in turn, causes changes in the plasmonic resonance frequency of gold nanodisks under the dielectric layer, which are read-off remotely with very high precision.

INPS sensor chips are nanofabricated by hole-mask colloidal lithography (17) of gold disks on glass substrate and are coated with a dielectric layer - often called spacer layer -which serves two purposes. One is to protect the nanoparticles from the direct contact with the reaction environment to keep their uniform response throughout the experiment. It also can be substituted with other dielectrics providing versatility and freedom to put different target materials on the sensor. The presence of the dielectric layer between the reaction environment and gold-disks as nano sensors imply indirect sensing. For the measurements the target material or reaction under investigation will be placed on top of the spacer layer. A schematic INPS sensor chip is shown in the figure 7 including the sample and experimental setup.

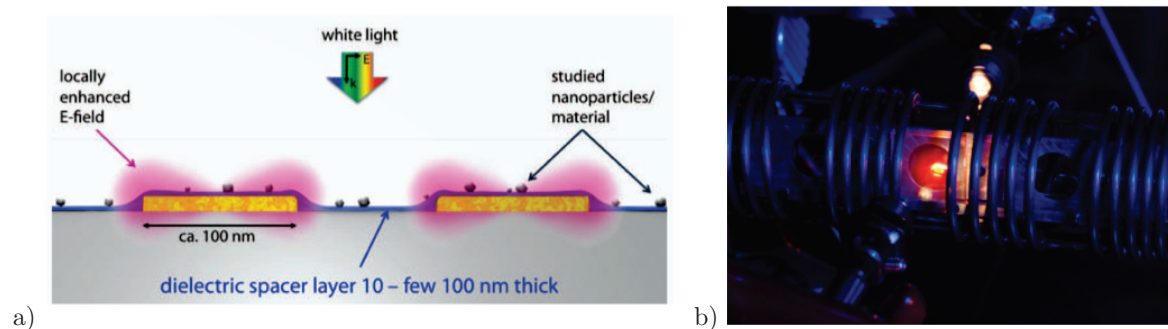


Figure 7- (a) Cross section of the sensor chip showing gold nanodisks and thin dielectric coating. The sample is placed on top of the dielectric layer and during the course of the reaction on the surface the plasmonic spectra of metallic nanoparticles is measured. (b) INPS sensor integrated setup with gas flow reactor experiment.

The sensor chip is integrated in a flow reactor to perform in situ studies at high temperatures and in controlled gas atmosphere. Transmission (reflection) of white light through (from) the reaction/process on top of the sensor is measured as absorption spectra by a fiber coupled spectrometer with high temporal resolution during entire time of the experiment. Different information such as plasmonic resonance frequency line width, extinction intensity and etc. are acquired. As an example for a measurement, a typical resonance shift from the INPS measurements during the sintering of a Pt/SiO_2 model catalyst in 4% O_2 and Ar, respectively, (18) is shown in figure 8.

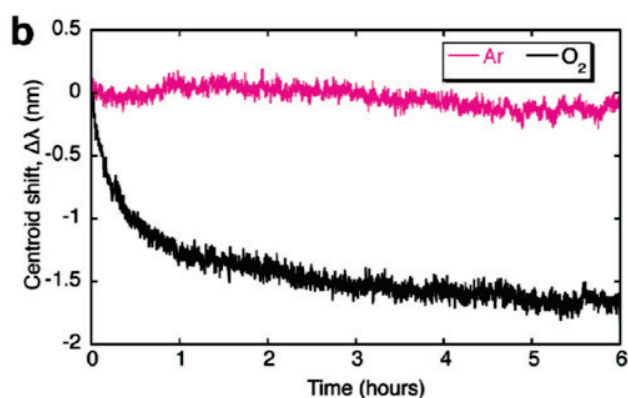


Figure 8- Blue shift of the resonance frequency (black curve) as a result of changes in refractive index induced by sintering of Pt nanoparticles deposited on the sensor.

In the first part of this work the sample deposition, standardizing procedures and their effects on the reaction will be discussed whereas in the second part of the work, the content will be devoted mostly to the kinetics and mechanisms of oxidation reactions measured by INPS under different highly controlled conditions.

References

1. The origin of soot in flames: is the nucleus an ion? V.J. Hall-Roberts, A.N. Hayhurst, D.E. Knight, S.G. Taylor. 4, *Combustion and Flame*, Vol. 120.
2. The oxidation of soot: a review of experiments, mechanisms and models. Stanmore, B.R., J.F. Brilhac, P. Gilot, s.l. : Carbon, 2001, Vol. 39, pp. 2247-2268 .
3. Ohlson, Carolin. Characterization of Carbon Oxidation Kinetics for Particulate Matter Reduction Technologies, Licentiate Thesis. s.l. : Chalmers University of Technology, 2010.
4. JB., Heywood. Internal combustion engine fundamentals. New York : McGraw Hill, 1990.
5. DONNET, J. B. STRUCTURE AND REACTIVITY OF CARBONS FROM CARBON BLACK TO CARBON COMPOSITE!3. s.l. : Centre National de la Recherche Scientifique, Centre de Recherches sur la Physico-Chimie des Surfaces Solides, 1981.
6. Soot oxidation: dependence upon initial nanostructure. Randy L. Vander Wal*, Aaron J. Tomasek. s.l. : *Combustion and Flame*, 2003. Vol. 134 , pp. 19.
7. Science and Technology of Catalytic Diesel Particulate Filters. Barry A. A. L. van Setten, Michiel Makkee,* and Jacob A. Moulijn. 4, *CATALYSIS REVIEWS*, Vol. 43, pp. 486-564.
8. A Random Pore Model for Fluid-Solid Reactions: 1. Isothermal, Kinetic Control. S. K. BHATIA, D. O. PERLMUTTER. 3, 1980, *AIChE Journal*, Vol. 26, pp. 379-385.
9. A Random Pore Model for Fluid-Solid Reactions. S. K. BHATIA, D. D. PERLMUTTER. 2, 1981, *AIChE Journal* , Vol. 27, pp. 247-254.
10. Development and validation of a model for the chemical kinetics of graphite oxidation. Mohamed S. El-Genk, Jean-Michel P. Tournier. 411 , 2011 , *Nuclear Materials*, pp. 193-207.
11. Zacharia, Renju. Desorption of gases from graphitic and porous carbon surfaces, PhD dissertation. s.l. : Freien Universitt Berlin, 2004 <http://www.diss.fu-berlin.de/2004/162/> .
12. Temperature Dependence on Structural, Tribological, and Electrical Properties of Sputtered Conductive Carbon Thin Films. al., Yong Seob Park et. 3, 2011, Vol. 32, p. 939.
13. C. N. R. Rao, A. Muller, A. K. Cheetham. *Nanomaterials Chemistry Recent Developments and New Directions*. s.l. : Wiley, 2007. ISBN 978-3-527-31664-9.
14. Nanoplasmonic Probes of Catalytic Reactions. Elin M. Larsson, et al., Christoph Langhammer, Igor Zoric, Bengt Kasemo. 2009, *Science Chemistry*, p. 1091.
15. Nanoplasmonic sensing for nanomaterials science. Elin M. Larsson, Svetlana Syrenova, Christoph Langhammer. 2012, *Nanophotonics*, Vol. 1, pp. 249-266.
16. Langhammer, Christoph. Nanoparticle Plasmonics in Classic and Novel Materials - Fundamentals of Hydrogen Sensing, PhD Thesis. s.l. : Chalmers University of Technology, 2009.
17. HoleMask Colloidal Lithography. Christoph Langhammer, Hans Fredriksson, Yury Alaverdyan, Alexandre Dmitriev, Duncan S. Sutherland, Michael Zch, and Bengt Kasemo. s.l. : *Advanced Material*, 2007, Vol. 19, pp. 4297-4302.
18. Real Time Indirect Nanoplasmonic in Situ Spectroscopy of Catalyst Nanoparticle Sintering. s.l. : *ACS Catal.* , 2012, Vol. 2, p. 2382-45.
19. Global and regional climate changes due to black carbon. Ramanathan, V., Carmichael, G. 2008, . *Nature Geoscience* 1, (), pp. 221 - 227.
20. Fine particles and human health: a review of epidemiological studies. Englert, N., s.l. : *Toxicol. Lett.*, (2004), Vol. 149, pp. 235-242.
21. www.Dieselnet.com.
22. Hydrogen Storage in Pd Nanodisks Characterized with a Novel Nanoplasmonic Sensing Scheme. Christoph Langhammer,* Igor Zoric, and Bengt Kasemo, Bruce M. Clemens. 2007, *Nano Lett.*, Vol. 7, pp. 3122-3127.
23. Indirect Nanoplasmonic Sensing: Ultrasensitive Experimental Platform for Nanomaterials Science and Optical Nanocalorimetry. Christoph Langhammer,* Elin M. Larsson, Bengt Kasemo, and Igor Zoric. s.l. :

ACS, 2010, Nano Lett., pp. 35293538.

24. Fifty years of reaserch and progress on carbon black. B., Donnet J. Mulhouse : In Second internation conference on carbon black, 1993. pp. 1-10. 25. HoleMask Colloidal Lithography. al, Christoph Langhammer et. s.l. : Adv. Mater, 2007, Vol. 19, pp. 42974302.

26. Differential kinetic analysis of diesel particulate matter (soot) oxidation by oxygen using a stepresponse technique. Yezerets, Aleksey. 61, 2005, Applied Catalysis B: Environmental , pp. 120129.

Chapter 3

Materials and Methodology

This section describes different experiments carried during the course of the project. It starts with a touch Printex U deposition on the INPS sensors and calibration with absorption spectra. It is followed by a short section on the synthetic soot oxidation in the INPS setup. The major part of the experiments is contained in the section for evaporated graphitic carbon samples and their subsequent isothermal oxidation experiments. In the last section, I demonstrate differential and sweep oxidation experiments.

3.1 INPS Sensor chips

A typical INPS sensor chip is shown in figure 1. It consists of a glass substrate on top of which an array of random and uniformly distributed gold nano-disks with diameter of 80 nm is nanofabricated by hole-mask colloidal lithography. The dielectric silica layer of 10 nm thickness is deposited by either sputtering or plasma enhanced chemical vapor deposition (PECVD). After fabrication, sensors were subjected to heat treatment (36-72 h at 600° C) for LSPR stabilization.

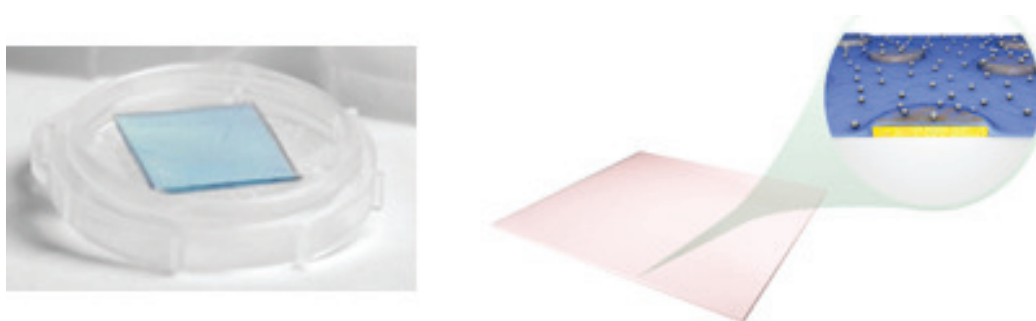


Figure 9 - INPS sensor chip with Au nanoparticles and coted with a 10 nm SiO₂ spacer layer (left) Schematic depiction of the sensor structure including nano-disks, spacer layer and material under investigation on top of spacer layer.

3.2 Deposition and Calibration of Model Soot

A good part the project time was spent on the first phase, i.e. attempting homogeneous deposition of Printex U model soot particles on the silicon dioxide layer of INPS sensor chips. Different physical and semi-physical methods were tested including pure powder of Printex U, spin coating, spraying and dropping dispersion solutions of Printex U on the surface of the sensors. Due to the generally poor results and adhesion obtained with all the tested methods, they are only briefly mentioned here and more details and results are provided in Appendix A.

3.2.1 Physical shaking method of Printex U model soot

In order to begin the study, the synthetic soot (Printex U) deposition on the sensor chips and its calibration was considered. The deposition and characterization method involved mechanically shaking of the soot sample with sensor chips, varying shaking times and soot amounts, measuring the absorption spectra by means of a spectrophotometer (Cary 5000) before deposition, with soot and after soot removal and try to correlate absorption peak shifts with shaking times and soot amounts. Soot removal consisted of sonicating the sensors in Aceton for 1 min and rinsing them with ethanol and blow dry with Ar. A combination of 5 shaking times (10, 20, 40, 60, 80 sec) and 4 soot amounts (0.005, 0.01, 0.025, 0.05 gr) were performed and each was repeated three times and average values of three repetitions were used.

3.2.2 Other Methods For Deposition of Printex U soot on INPS sensor chips

From poor results of mechanical shaking, other deposition methods such as spin coating and spraying of Printex U solutions were tested. Different suspensions of Printex U including in ethanol, acetone, dichloromethane and water-ethanol mixtures were tested. The best solvent seemed to be acetone. Normally a colloidal suspension formed with aggregated particles, which even after sonication up to 10 minutes could be considered quite inhomogeneous. Sedimentation occurred after few hours. Variations of spin speed and accelerations did not seem to influence the deposition uniformity, as checked with optical and electron microscopy. Images are included in the appendix A section. The same suspensions were also used to spray the soot on the sensor by means of a commercial airbrush. Variation of spray time and suspension concentration was tested and evaluated with SEM images. Another method tested, consists of dropping a highly concentrated and sonicated dispersed suspension of printex U on the sensor chip and simply letting it dry off. As a result a thick and uniform layer of black printex U was formed, which, during the consequent oxidation experiment, flew off the surface as big flakes due to the cracks resulting from shrinkage during drying.

3.3 Carbon film deposition

Due to the poor attachment of the Printex-U on the sensor chips and, as a result, weak output signal in the isothermal oxidation experiments, graphitized carbon was instead selected and deposited on the sensor chips which previously had shown uniform and good attachment with a good detectable signal. Deposition was done by electron beam evaporator (AVAC) at the clean room facility at MC2 Chalmers. In each deposition badge, 8-9 sensor chips were mounted and thin graphitized carbon films with nominal thicknesses of 5, 10 and 30 nm were evaporated for different experiments and always on the same 9 sensors.

3.4 Measurement Signals

Basically in all oxidation experiments in this thesis, the absorption spectra taken during the experiments, are laying in the spectral range of 400 -800 nm. Two main signals were specifically chosen and tracked from the absorption spectra. The first one is the plasmonic peak shift and the second one the light extinction intensity at 800 nm. After deposition of the carbon film on the sensor chips, the measured absorption spectrum is the convolution of the both LSPR and the carbon film absorption profile, which increases toward UV region. In order to decouple these two spectra and to be able to only measure the absorption associated with the carbon film, it is best to move toward the IR region where the LSPR has almost no response. Hence the remaining absorption is a direct measure of amount of carbon thickness present on the surface.

3.5 Carbonaceous Matter Oxidation Studies with INPS

3.5.1 Printex U Step Response Oxidation

Isothermal oxidation of Printex-U deposited on the INPS chips by the physically shaking method were performed at 550° C and at 2 vol.% oxygen in an Insplorion X1 (Insplorion AB, Gteborg, Sweden) flow reactor system. Results are presented in the appendix A.

3.5.2 Step-Response oxidation of Graphitized Carbon

For a major part of the experiments, graphitized carbon film oxidation in isothermal fashion was performed to extract a complete set of data for kinetic analysis. In doing so, four different temperatures of oxidation 450°, 500°, 550°, 600° C and also three different oxygen concentrations of 0.5, 2 and 21 vol. % were chosen to examine a broad range of oxidant availability and connected to technical relevant conditions with each experiment being repeated twice. In total this constitutes twelve different combinations for the purpose of acquiring a complete set of data for kinetic analysis. For this block of experiments films of 5nm thickness were used. In all experiments with constant oxygen concentration films deposited in one deposition session were used, i.e. they should be identical. Since the INPS setup is capable of measuring on two samples simultaneously in the reactor, always, next to the carbon loaded sensor, a blank sensor was placed upstream to measure just the mere response of sensor to the reaction environment. Isothermal experiments involved heating the sample from room to target temperature of oxidation at approximately 45–60° C/min, depending on the destination temperature, under inert atmosphere of high purity Ar, maintaining the temperature for few minutes, which was followed by an oxygen step as the main part of the experiment. A schematic of the step-response oxidation is illustrated in figure 10.

Later, oxidation of the 10 nm films with only one oxygen concentration (21 vol.% O_2) and at previously mentioned different temperatures were performed for comparison. In order to check for the setup related variations, isothermal experiments with only one sample in the reactor and with two samples in the same reaction environment were run and the respective results were compared.

3.5.3 SEM Imaging of the carbon films

From the results of the isothermal oxidation experiments on evaporated carbon films (showing significant variations in reactivity of nominally identical carbon samples) it was concluded that SEM investigation of the deposited films is needed for further evaluation and to explain some of the observations described in detail in the result and discussion section. Since 5nm films were not yielding good contrast in the SEM, 10 nm thick carbon films were deposited on all 9 sensors and successively SEM images were taken. Moreover, also films with 30 nm thickness SEM images were taken for a comparison and qualitative evaluation. In order to check the reproducibility of the oxidation data for 10 nm films, they were all subject to the identical isothermal oxidations at 450o C and 2 vol.% O_2 . The result is presented in the next chapter.

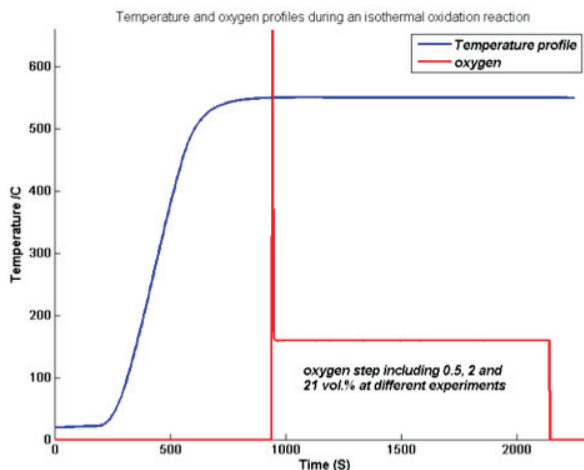


Figure 10 - Illustration of a typical the step-response oxidation used to extract a complete set of data. At different experiments specific target temperatures and oxygen concentrations were used.

3.5.4 Sweep Experiments

The step-response experiment exhibited a very poor reproducibility due to a number of reasons such as variations of reactivity, thermally-induced microstructural changes and uncontrolled self-heating effect during progressive oxidation among different samples. In order to be able to extract comparable data, as is crucial for the targeted kinetics analysis, and to also minimize the variations associated with the carbon films in different samples, the shortest and best solution was to be using only one sample and to, instead of isothermally oxidizing it to full conversion, differentially oxidize it at different temperatures and oxygen concentrations. This assumption allows for measuring the reaction rate at nearly constant conversion, which renders conversion-independent data for a global kinetic analysis. This also implies that rate determining factors associated with the physical and chemical structure of the graphitic film are essentially the same for the whole set of data.

Based on the mentioned description, an experiment was designed for a sample comprising a 30 nm thick carbon film including oxidizing the sample differentially (differential in terms of carbon conversion %) via a sequence of oxygen pulses (in this case 3, 6, 10, 13, 16, 20, 25 vol.%) each separated from the subsequent one by two minutes of Ar flow at a constant temperature. The same procedure was repeated at different temperatures in the following order: 405°, 454°, 504°, 529°, 479° C. The last temperature step in a decreasing manner, opposing to the increasing trend of previous steps, was used to study thermal history effects on the resulting kinetics.

In order to exclude the effects of highly active surface compounds and adsorbates to the determined reaction rate, prior to the oxidation sweeps a Temperature Programmed Desorption (TPD) step (21 – 600° C at a heating rate of 5°C/min) succeeded by maintaining sample temperature at 600° for 20 minutes was performed. This TPD step was then followed by introducing a "light" oxidation step to just oxidize highly active surface compounds under the condition of T=450°C and 3 [vol.%] O₂ for 4 minutes. After these sample pretreatment steps, the oxygen sweep experiments were performed in the mentioned order. Using the so-obtained oxidation rates and the global rate equation as kinetic model, it was aimed to calculate the reaction order of oxygen. A schematic of the experiment design is presented in the figure 11.

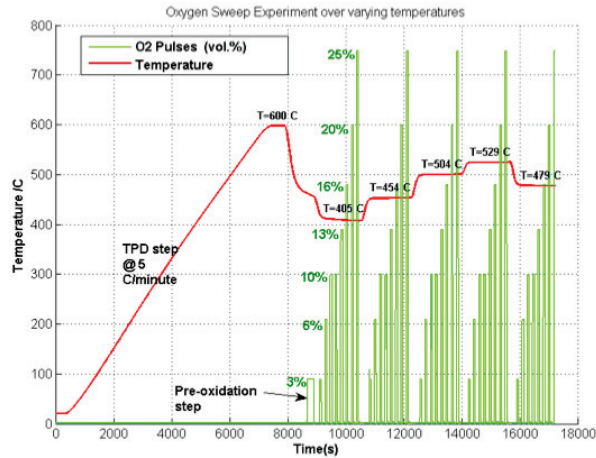


Figure 11 - Oxygen sweep oxidation schematic including pretreatment, temperature profile and oxygen pulses.

3.5.5 Conversion Dependence of the Reaction Rate

The last experiments were designed in order to better understand the behavior of a carbon film during oxidation. A nominally 30 nm thick carbon sample was chosen, which was around 1 month old. An experiment was designed and performed as a series of oxidation pulses at constant temperature and constant oxygen concentration throughout the whole carbon conversion. A TPD step prior to the first oxidation was added from room temperature to 600° C at 10° C/min in Ar. The oxidation temperature was chosen relatively low, about 410° C, assuring the reaction condition completely free from mass transport limitations.

An O_2 concentration of 10 vol.% in Ar as carrier gas was kept for all oxidation steps. The whole experiment is divided into 12 identical blocks which are numerated, each being separated from the subsequent one by few minutes in Ar. Each block also consisted of 5 oxidation pluses of 30 sec each and separated by 2 minutes from each other. The experiment design and is shown in figure 12 for all oxygen and temperature conditions of the experiment.

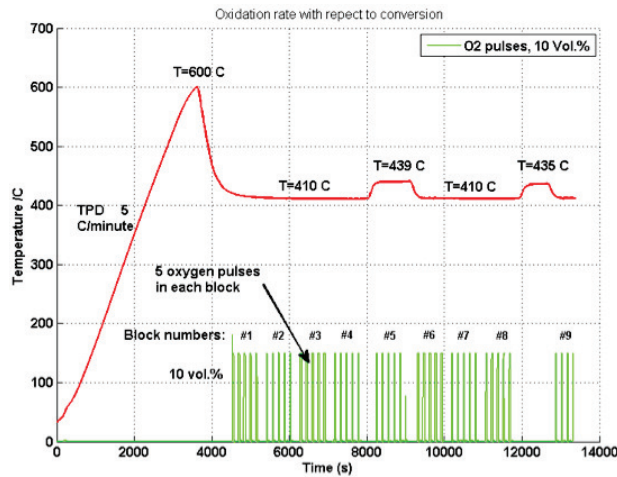


Figure 12 - O_2 pulses and temperature plateau during the experiment are depicted in arbitrary units. Blocks are numbered and the resulted extinction signal of each block is vertically shifted down and separately drawn below the temperature for ease of qualitative comparison.

Chapter 4

Results and Discussions

In this chapter, results of non-catalytic carbon film oxidation experiments with O_2 measured by the INPS platform (description of which is mentioned in earlier chapters) are presented. It will include isothermal, oxygen sweep and differential oxidation experiments. For specially the isothermal block, a selection of result is presented and outcomes from experiments of synthetic soot are separately displayed in the appendix A.

4.1 Isothermal Oxygen Step-Response Experiments

4.1.1 5 nm thick films

Series of isothermal oxidation experiments of 5 nm carbon films over a range of temperatures and particular oxygen concentrations are plotted in panels of figures 13 for three different oxidant concentrations of 0.5, 2 and 21 vol.%, respectively. Each experiment was repeated twice and data represent only the oxidation intervals of the experiment time and are normalized to unity for both signals, i.e. plasmonic peak shift and extinction intensity at 800 nm. As the extinction signal is indicative of the carbon load on the sensor, the rate at which it reduces is connected to the removal of the carbon from surface, i.e. the rate of oxidation. As expected, the general trend of rates at different temperatures at fixed O_2 concentration, as can be seen, is that with increasing temperature the rate also increases which results in vanishing the extinction signal quicker. However, in some of the experiments, this trend does not hold and for two nominally identical repeated experiments, the rates are not overlying each other despite identical reaction conditions.

Since for each of the panels in figure 13, i.e. at each oxygen concentration, the films were evaporated in the same session, they are expected to be of the same physical and chemical properties and therefore reactivity towards oxidation. Yet for some of the cases mostly toward lower temperature, the reproducibility becomes significantly much worse.

4.1.2 10 nm thick films

A series of isothermal oxidations similar to those for 5 nm thick films was repeated for films of 10 nm thickness only at 21 vol.% O_2 concentration for comparison and determining the thickness effect. The oxygen concentrations were chosen such as to avoid any mass transport limitation by guaranteeing oxidant abundance. Oxidation profiles are plotted in figure 14 top panel. Regarding the reproducibility there are evident outlier curves which tend to become worse at lower temperatures. A comparative graph of 10 and 5 nm films are displayed in figure 14 lower panel. As it can be seen, the general trend of higher rates at higher temperatures is seen but not for all samples. In some cases the oxidation time is almost the same for both 5 and 10 nm films under same reaction environment which is unexpected since the carbon load is different.

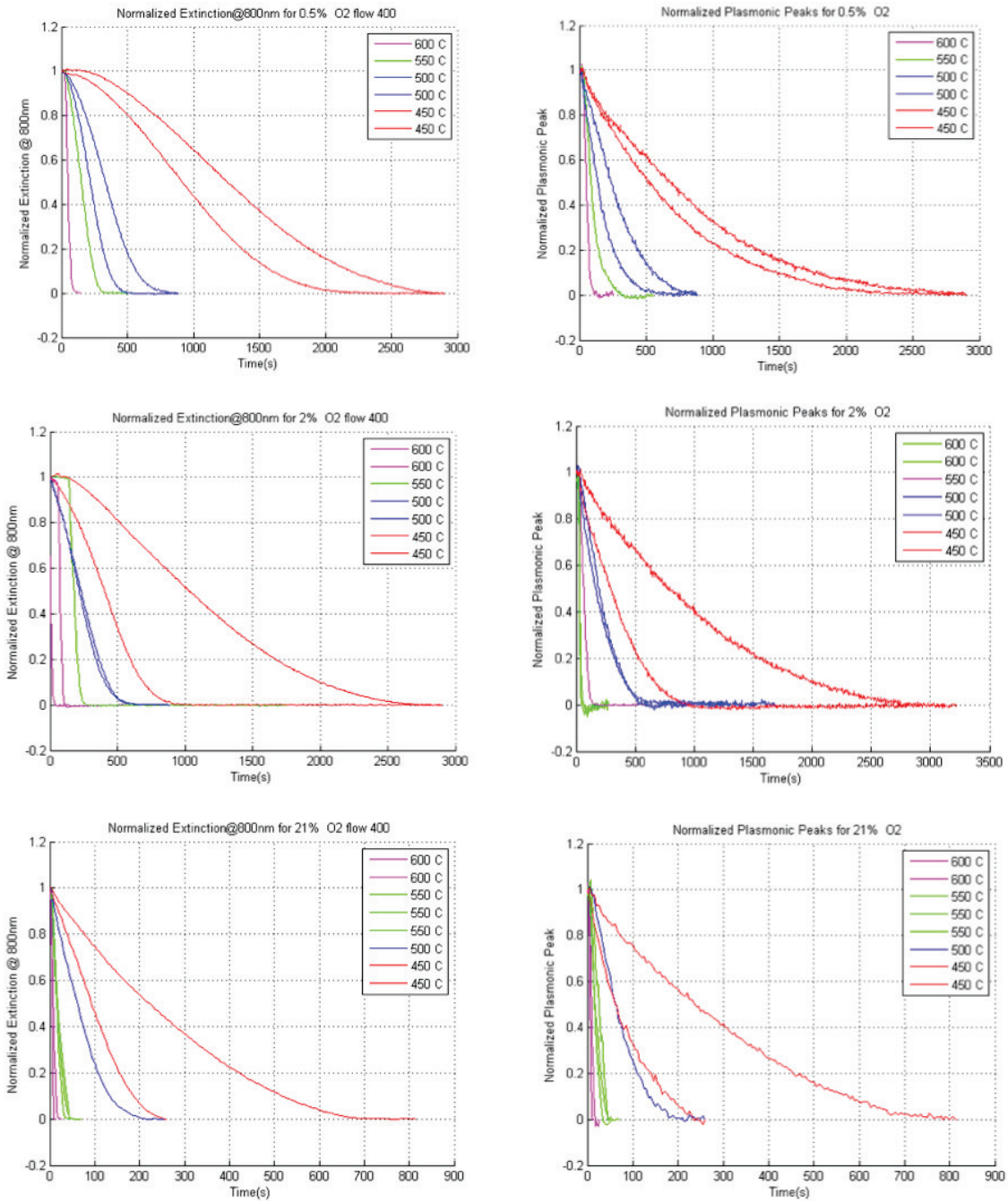


Figure 13 - Isothermal Oxidation of 5 nm carbon films result under three different Oxygen concentrations of 0.5 vol.% (top panel), 2 vol.% (middle panel) and 21 vol.% (lower panel), each at four different temperatures are shown in the graphs. The left column of graphs is the extinction at 800 nm signal and the right column is the plasmonic peak shift in nm, both normalized to unity. Each experiment has been repeated twice for reproducibility observation.

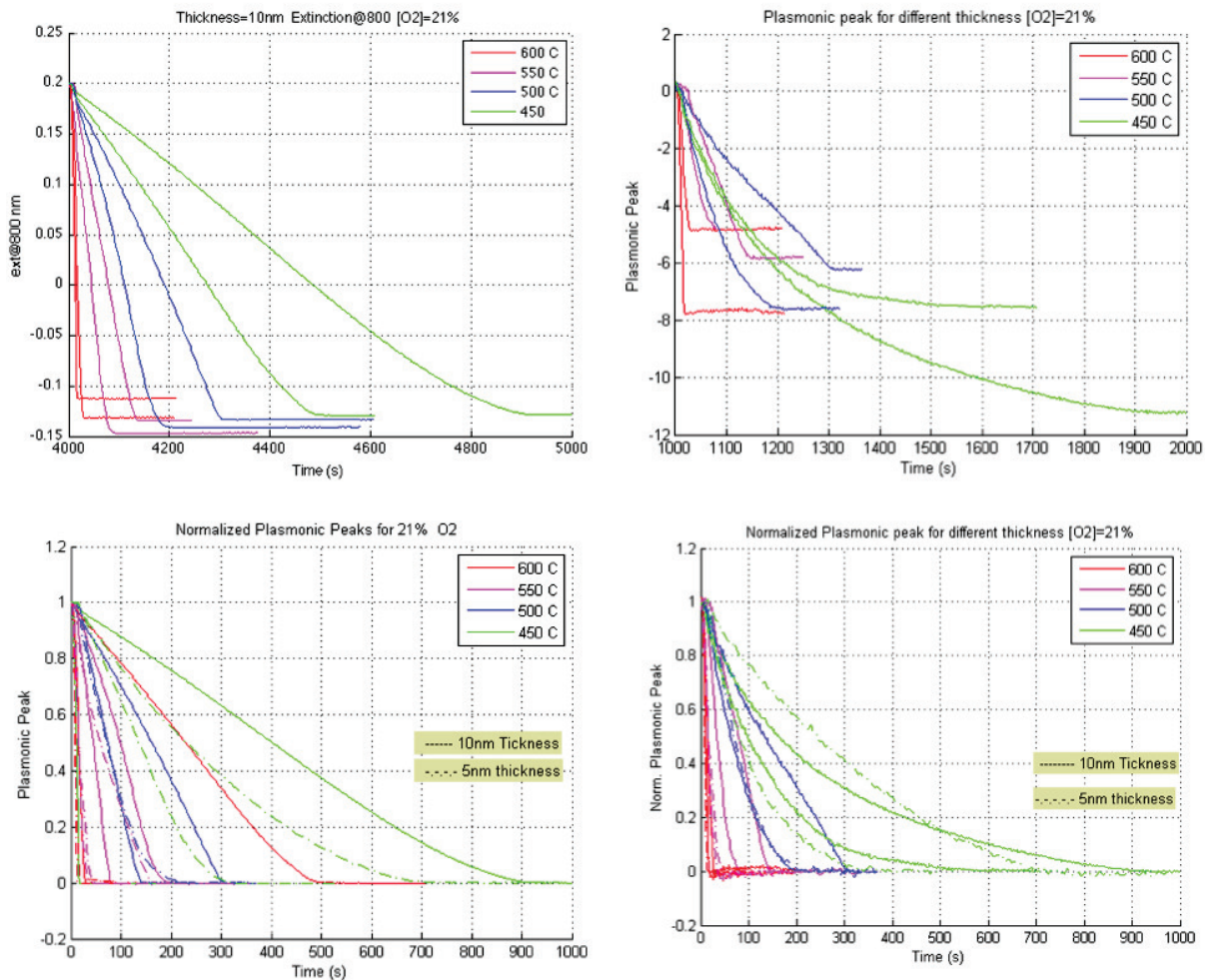


Figure 14 - Extinction signal (left) and plasmonic peak shift (right) are presented in the top panel for 10 nm carbon film isothermal oxidation at 21 vol.% oxygen concentration and various temperatures. In the lower panel normalized extinction signal and plasmonic peak for both 5 and 10 nm films are plotted for a comparison.

Extinction signal which is representative of carbon load on the sensor are different in various experiments despite that they, ideally, should be the same. This difference could be attributed to a number of reasons such as uncontrolled pre-oxidation of samples at higher temperatures in the reactor before the oxidative step and the fact that initial value of the extinction signal increases for increased temperatures. A variation also could come from the deposition step resulting in minute difference in thickness of the films which could be ignored due to the apparatus and precision of deposition. In connection to the plasmonic sensors, parts of the seen variations in plasmonic peak signal could be due to the different sensitivity of the different sensors to the same reaction. Also both signals are influenced by the temperature they are recorded at so comparing different temperature results should be studied carefully. For the mentioned reasons and also due to more complex nature of plasmonic peak signal and its dependency on other factors such as distance of the phenomenon from the sensor surface (1), for the rest of the experiments and specially the kinetic analysis, only the extinction signal was considered. Considering the mentioned points above, film thickness variations, i.e. the total shifts of the extinction signal for both 5 and 10 nm films during oxidative step, can be seen in the results of INPS (figure 15).

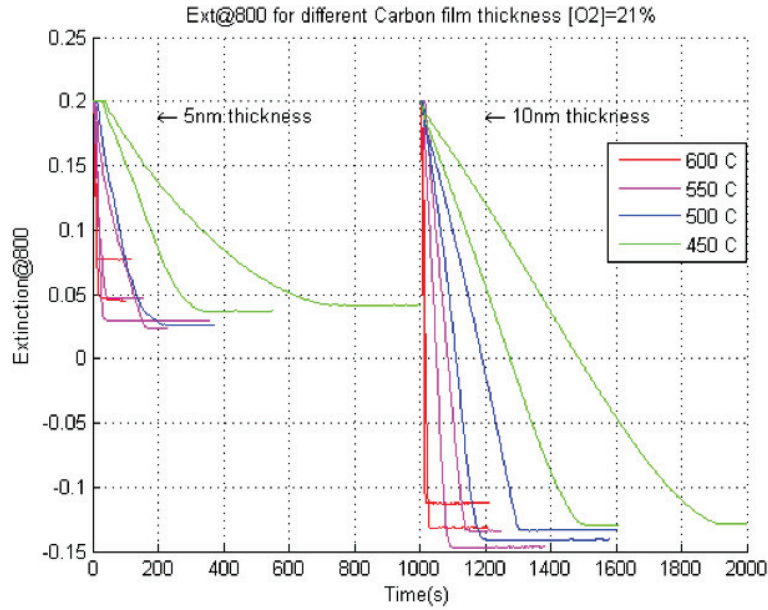


Figure 15 - Comparison of total extinction shift induced by oxidation of 5 and 10 nm films isothermally and under 21 vol.% oxygen. The average total shift of the 10 nm film is almost twice that of the 5 nm films which is expected.

4.1.3 Double channel oxidation

In order to minimize the potential variations of the reactor setup from experiment to experiment, and to check the origin of irreproducibility, a number of experiments was carried out with two samples simultaneously in the reactor in abundance of oxygen (21 vol.%) to avoid oxidant deficiency, and at different temperatures of 500°, 550° and 600° C. This arrangement is opposite to the previous isothermal experiments up to this point where only one sample was oxidized at a time. The resulting extinction signals are shown in figure 16.

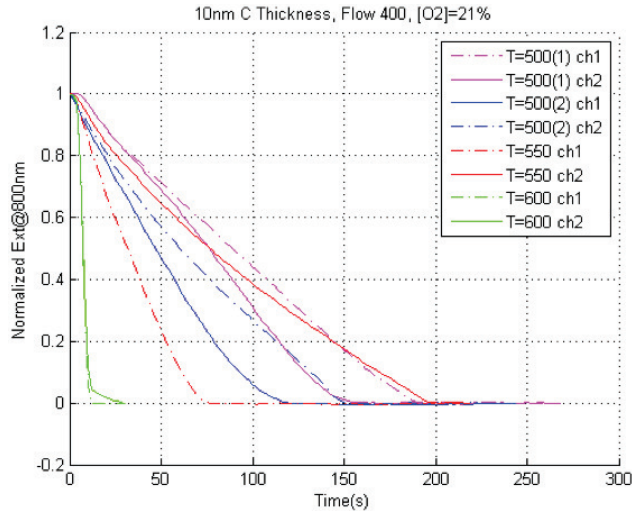


Figure 16 - Results of 4 different double-channel experiments. Normalized extinction signal from simultaneous Isothermal Oxidation of two samples in the reactor for different temperatures and in 21 vol.% oxygen. Oxidation at T=500° C is repeated twice. As can be seen in the double channel experiments for the same reaction environment and for the samples similarly prepared, different oxidation rates are observed.

SEM Analysis: In the search of origins of different oxidative behavior of the samples micro analysis of the samples with ESEM was aimed for. Firstly films of 10 nm thickness were investigated, however, a clear trace of carbon films was not observed. The same investigation was then repeated for freshly produced 30 nm thick films and it was tried to maximize magnification. A selected result of different film thicknesses are shown in the figures 17 and 18. The large hexagonal-like particles are gold nano particles and the carbon can be seen as a spread of smaller gray and blurry dots all around the surface. As can be seen carbon forms clusters on the surface and in the case of 30 nm films, the average size of clusters and their density is higher as compared to the 10 nm films. After taking SEM images of 10 nm-thick films, all evaporated in the same badge, they were used in 9 similar oxidative experiments to check for the reproducibility in terms of oxidation rate. The conditions were chosen as low as $T = 450^{\circ} \text{C}$ in order to avoid any dominance of oxidation over diffusion of oxygen and $\text{O}_2 = 2 \text{ vol.}\%$. Results of similar step response oxidations are plotted in the figure 19 for the extinction@800nm signal. As is evident in the figure, the variations of the rate from one experiment to another are rather rough and this consequentially shadows the reliability of the complete set of oxidation experiments with 5 nm films.

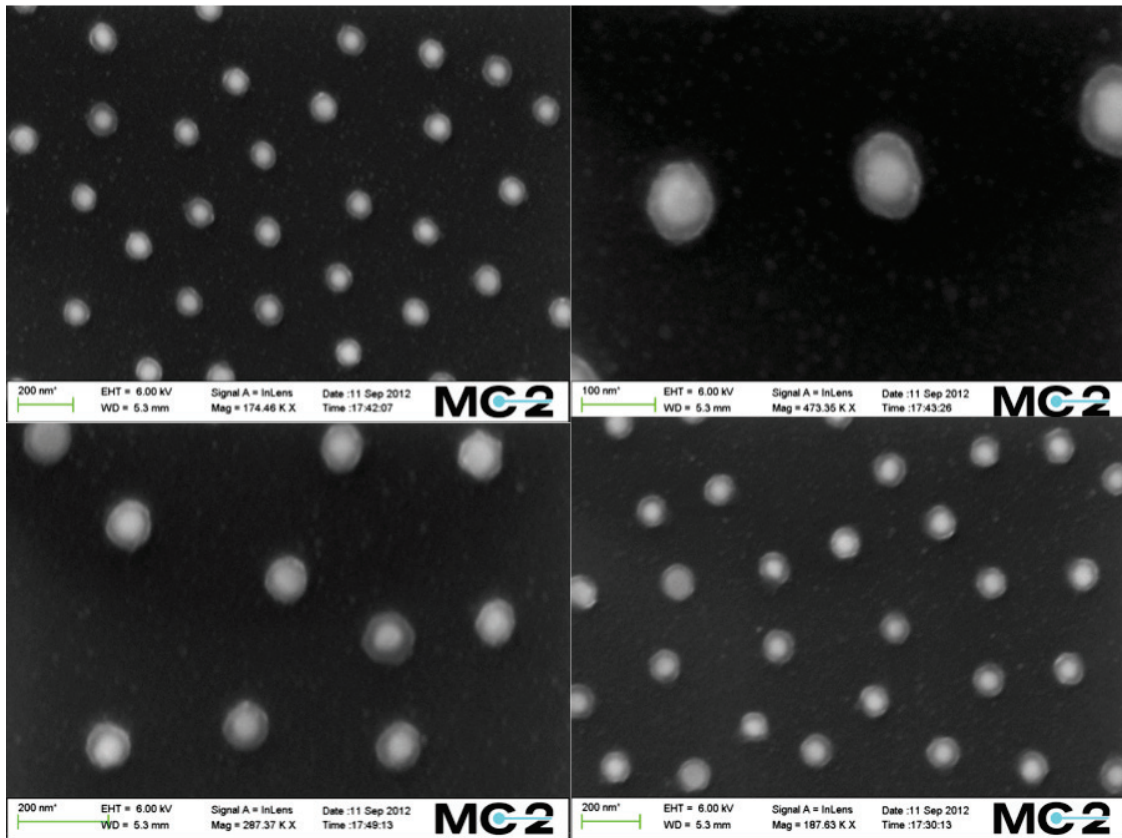


Figure 17 - SEM images of the 10 nm thick carbon films deposited in the same deposition batch.

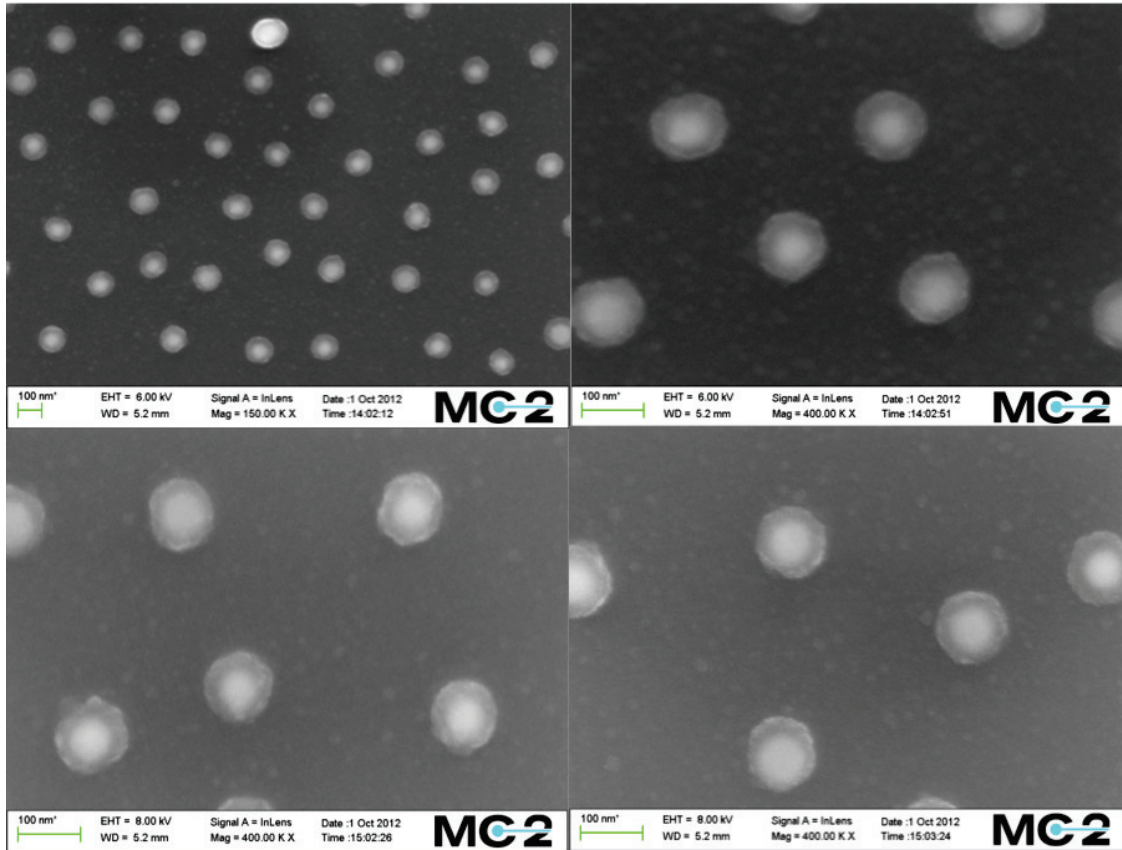


Figure 18 - SEM images of the 30 nm thick carbon films deposited in the same deposition batch.

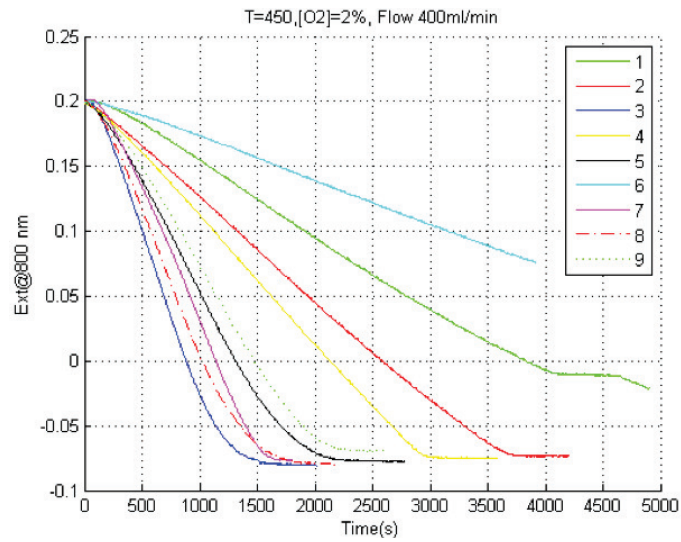


Figure 19 - Isothermal oxidation of 10 nm carbon films under T= 450 C and 2 vol.% oxygen repeated for all 9 samples.

As discussed above, the variations are thought to be mainly attributed to the different properties acquired during the deposition step of the carbon onto the sensors and the oxidation condition, which will be addressed in the discussion section.

4.1.4 Activation energy estimation in the Arrhenius coordinates

In order to kinetically evaluate the series of step response isothermal oxidation data, they were used in the Arrhenius kinetic formalism to estimate the activation energy for the oxidation of the graphitic carbon films. According to the rate equation as discussed above we have:

$$r = k(T) \times [C]^\alpha \times [O_2]^\beta$$

And normalization of reaction rate equation gives the following form:

$$\frac{r}{[C]^\alpha \times [O_2]^\beta} = k(T) = Ae^{-E_a/K_B T}$$

Now if we write reaction rate as inverse time of a certain oxidation during each of the experiments as a rate representative and re-plot the data, its possible to estimate the activation energy in the Arrhenius coordinates:

$$\ln(r_{Normalized}) = \ln(A) - E_a/K_B T$$

The result of the data from step response experiments come in the following graph 20:

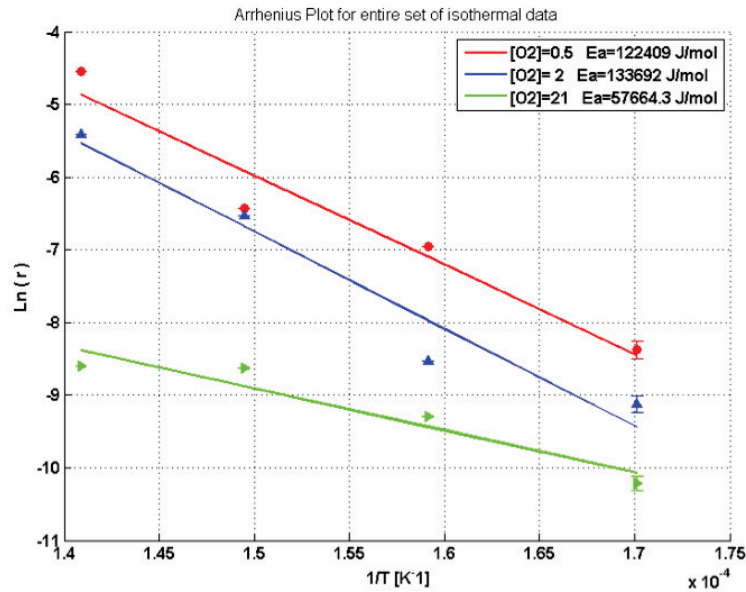


Figure 20 - Activation energy estimation for isothermal oxidation series.

Error bars on the plot are propagated errors coming from measurement precision of time intervals calculated from the following general rule:

$$\begin{aligned} \delta Q &= | da/dx | \\ Q &= \ln(1/t) \\ \Delta Q &= \left(\frac{d}{dt} Q \right) \Delta t = \frac{d}{dt} \ln\left(\frac{1}{t}\right) \Delta t = \frac{1}{t} \Delta t; \Delta t = 2s \end{aligned}$$

According to the results of the step-response isothermal oxidations of 5 nm thick carbon films within a range of temperatures and oxygen concentrations, it can clearly be seen that reproducibility is low and to some extent seemingly random. Also the trend of the oxidation rates does not completely follow the higher rates at higher temperatures. There is a number of factors that could contribute to these observed results: During the course of the graphitic carbon oxidation, as the exothermic reaction is progressing, the generated heat of the burning can add up to the temperature of experiment and as a result promote higher rates. The longer the experiment time is, the larger is the extent to which two identical experiments can differently proceed due to the uncontrolled heat. An evidence for this is that generally the deviations in reproducibility are higher at lower temperatures and oxygen concentrations (figure 21) in which the time of experiment is longer for the full conversion. Temperature control of the samples during the oxidative step, support that temperature raise during some of the oxidations can build up to around 10 degree where for experiments carried at 600° C, is around 4 degree Celcius as shown in the figure 21. Also temperature raise versus time of oxidation is demonstrated in figure 22. In other experimental situations such as for synthetic soot, this could be avoided by diluting soot with higher thermal capacity materials such as SiC chips (2) as heat sink which was not possible to do with carbon films. Regarding the homogeneity of the carbon material, from the findings in the soot oxidation studies the inhomogeneity in the material normally causes sudden spikes in the oxidation profile (2) and for the graphitized carbon film this can be tested with temperature programmed oxidation for a better qualitative understanding of the oxidation behavior. However, it does not seem to matter for the carbon source used in this study and also for the temporal averaging principle of measurement technic used in INPS.

Additionally, different graphite microstructure formed during the deposition of films in different samples and reactivity changes in thermal treatment during experiment could play a part in oxidation behavior variations. Moreover, in the thermal annealing of the carbon nanoparticles (the same commercial source as the carbon films of this project) in another unpublished work done in our group, at temperatures ranging from 400° – 800° C, consequent SEM image analysis has shown increased degree of crystallinity and structural changes of the particles after 10-20 minutes, as is also explored in (3). As reactivity of carbon material is connected to the concentration of defects and edge planes (4) & (5), mentioned ordering could result in a decreased number of active sites and thus suppressed reactivity, which can be significant for the lower temperature oxidations as carbon resides longer time in the reaction temperature, e. g. 30 -60 min which induces more restructuring over the conversion. Active surface area of carbon during oxidation is known as the most puzzling feature of its oxidation reaction. It is known for the carbon that the active surface area during the progressive oxidation changes as is discussed in the introduction section and for example (4), the reaction rate must be normalized with a function representing the active surface area for a conversion independent rate. As such function needs to be estimated by other experiments like BET measurements and is not applicable to the carbon films samples by available equipment, this is unknown for the samples and makes the comparison of the rates more controversial. In order to measure any issue relating to transport phenomena in the carbon oxidation, combustion regimes of oxidation must be identified (6). Nonetheless, external transport limitations could be ignored due to the design of setup and samples. Also internal transport limitations (restricted diffusion) do not seem to be an issue here due to the very thin thickness of the films i. e. 5 or 10 nm. Were it to be so, diffusivities as low as 510-9 m^2/s must be in effect. Additionally, a diffusion limited process should be accentuated at higher temperatures where the reaction rate could outstrip the diffusion whereas among isothermal oxidation series performed here the most deviations in reproducibility are observed at the lowest temperatures.

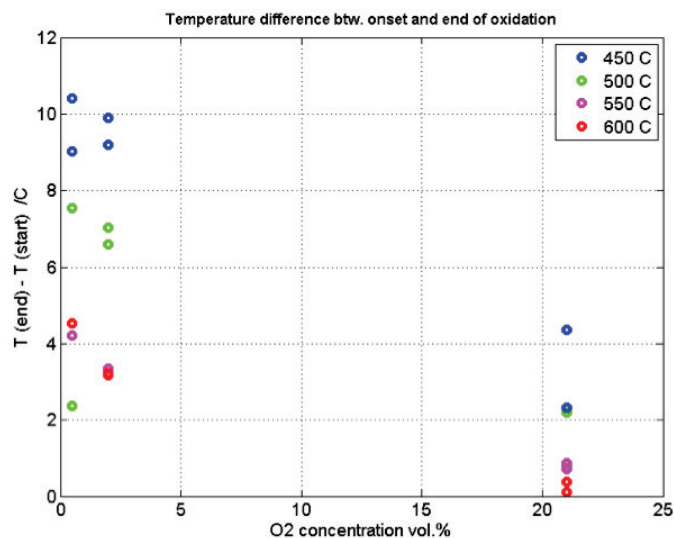


Figure 21-Temperature raise during the oxidative steps of the isothermal oxidations at different oxygen concentrations.

It is well known about the carbon material that overnight exposure of the carbon to the ambient condition results in the adsorption of species such as water and hydrocarbon and arguably formation of the reactive solid carbons as is investigated in (7). Adsorbed species can be desorbed during a Temperature Programmed Desorption (TPD) prior to oxidation yet reactive stable surface groups might remain in the sample causing initial high but rapidly decreasing reactivity in the oxidation profile. Since effects as such are only present in the initial stage of the oxidation, for a prolonged continuous oxidation they dont seem to be of significant influence. Yet it should be noted that for some of the short experiments such as oxidations at 600° C taking around few seconds to minutes this could be important. To summarize, from these experiments it is concluded that this set of isothermal oxidation data is not of high enough quality and thus not reliable for the purpose of the kinetic analysis. Consequently it cant be used for concluding the usefulness of INPS technique in this context. This, though unfortunate, motivated another range of experiments which seemed more promising in carbonaceous matter oxidation studies. As a project extension, further experiments were designed and performed which are presented in the next heading.

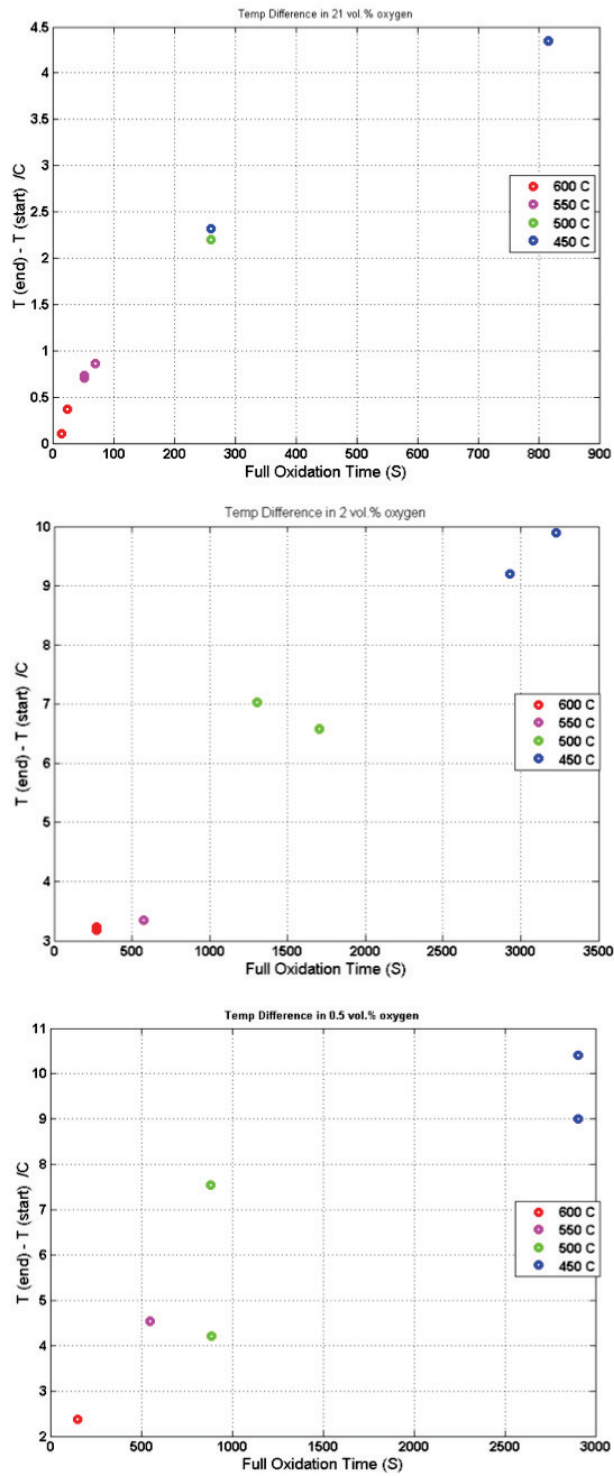


Figure 22 - Temperature raise during oxidation versus time of the oxidation and for different temperatures and oxygen concentrations: 21 vol.% oxygen (top panel), 2 vol.% oxygen (middle panel) and 0.5 vol.% (lower panel). It is evident that for the longer experiments i.e. lower T and oxygen concentrations the temperature raise is higher.

INPS coupled with Mass Spectroscopy: In order to compare and correlate the results from INPS with conventional mass spectroscopy technique, a mass spectroscopy analyzer was connected to the downstream of the reactor during a number of Isothermal oxidations. Among the observed species by the detector, the CO and CO_2 signals which are the primary and main product of the oxidation, exhibited a very weak signal which was thought to be due to the very low load of carbon and sensitivity limit of the mass spectrometer. Long after the setup was removed it was revealed that there has been a problem with the signal amplifier rendering very weak signals which was not so fortunate. Hence this part left unaccomplished.

4.2 Oxygen Sweep Experiments

4.2.1 Oxygen reaction order

In order to overcome some of the problems associated with irreproducibility between different samples, a new and different oxidation strategy was considered. This technique, which is based on the isothermal oxidation of the carbon only *differentially* compared to the full load of carbon, and as opposed to the continuous oxidation, allows for decoupling several effects influencing the oxidation reaction, such as conversion dependencies (8). Additionally oxidizing small amount of carbon allows for minimized thermal effects pertaining to the self-heating which previously was shown to induce rough deviations in the oxidation profile reproducibility.

Based on this, differential oxidation of one sample by a series of oxygen pulses was designed and performed to analyze quantitatively the kinetics. This is realized by assuming that the carbon reaction order does not change during a differentially small oxidative step. Then we could renormalize the rate equation as in the following:

$$\frac{r}{[C]^\alpha} = k[O_2]^\beta$$

By spanning a series of oxygen pulses on a single sample and sweeping a range of oxygen concentrations at constant temperature, it will be possible to measure r and O_2 and fit for the β parameter. The same procedure can be repeated at different temperatures to map r over different temperatures and conversion degrees over the same sample. 30 nm thick carbon films and a sequence of oxygen steps (3, 6, 10, 13, 16, 20, 25 vol.%), each separated from one another by 2 minutes of inert Ar flow at a constant temperature were used. The same procedure was repeated at different temperatures in the following order: 405°, 454°, 504°, 529°, 479°C. In order to exclude the effects of highly active surface compounds and adsorbates from the reaction rate, a TPD step was added in the range of 21 – 600° C at 5°C/min in the beginning and succeeded by maintaining the sample temperature at 600° for 20 minutes. This was followed by introducing a short oxidation step to just oxidize highly active surface compounds under the condition of T=450° C and 3 [vol.%] O_2 for 4 minutes. In the following graph (figure 23) the result of the experiment is presented for the oxidation periods.

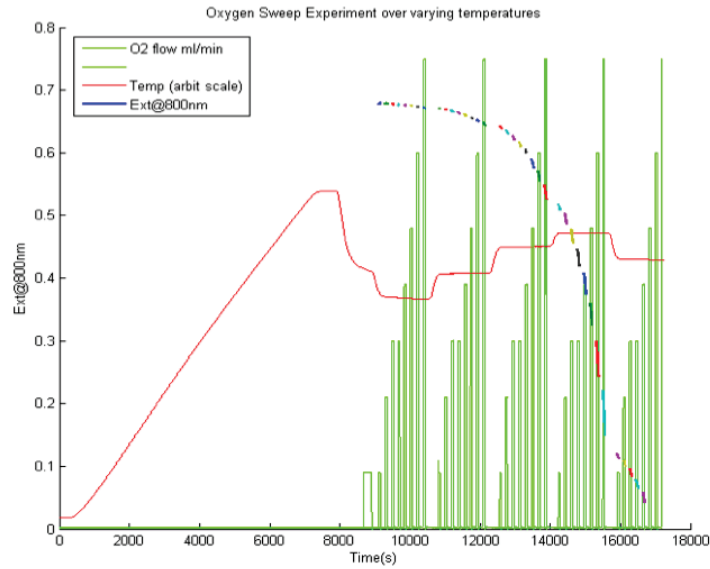


Figure 23 - Oxygen sweep experiment result including oxidation conditions parameters. Colored dashed curve is the extinction signal during each oxidative step.

In the following, an oxygen reaction order estimation based on the kinetic model mentioned above and in the order of the performed temperature is presented in the figure 24. The rate constant, i.e. the k factor for the calculations, should by definition be constant for isothermal and iso-conversion condition, Hence it should not influence the obtained oxygen reaction order at constant temperature and is thus assumed to be constant during one oxygen sweep. However, it should be noted that for the oxygen sweeps at higher temperatures, as the conversion changes more significantly during a single oxidative pulse, which consequently could result in changes of A (pre exponential factor within k), the rate should be normalized by the available carbon to compensate for k . The result is shown in the following graph:

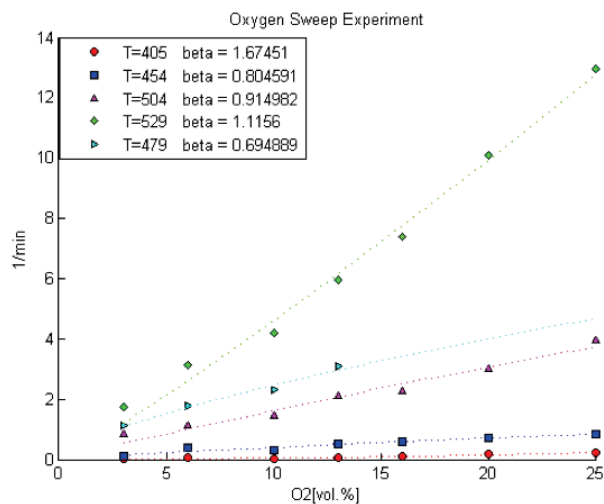


Figure 24 - Oxygen sweep experiments and estimated oxygen reaction order corresponding to their respective temperatures. The order of the temperatures from top mimics the cycles during experiment.

The oxygen reaction order data corresponding to the temperature and conversion are summarized in the table 2. It can be seen that the reaction orders, except from the one obtained from the first sweep the temperature of which might be low for a considerable reaction rate, are within the proximity of one which is generally expected for the oxygen reaction order and also reported values in literature. See for example (8). The rather large reaction order of the oxygen during the first sweep could be ascribed to the high surface coverage of oxygen formed during pre-oxidation step at temperature of 375 C, which might be low for desorption to occur. From the scatter of the beta over the temperature range no immediate correlation can be found between reaction order and temperature which this has also been observed in other studies of Printex U (8). This variation of the reaction order at different temperatures could originate from a number of reasons. It might be due to the conversion, carbon surface chemistry and surface complexes, mechanistic pathways and rate determining steps which could vary due to the temperature and history that sample has been through. Considering proposed mechanisms of Eley-Rideal and Langmuir-Hinshelwood (5) as two main mechanisms for the carbon oxidation. one of the possible scenarios could be that lower than one reaction order exhibits saturated coverage for the impact and reaction scenario of ER and higher than one reaction order could mean activation of more stable surface oxides existing on the surface from interaction with oxygen supplied by bulk gas or from surface of solid through Langmuir-Hinshelwood mechanism. The highest reaction order obtained in the first sweep at 405° C i.e. the lowest temperature cycle throughout the experiment, could be due to the presence of highly reactive surface compounds remaining after TPD and peroxidation steps. Moreover, adsorption dependence on the oxygen partial pressure, desorption rate as a function of temperature, reaction rate as a function of various reaction steps and temperature, all could contribute to the variations in reaction order of the oxygen.

Order of T step	Temperature (1/C)	Beta
1	405	1.67
2	454	0.8
3	504	0.91
4	529	1.11
5	479	0.69
	Average	1.03

Table 2 - The beta parameter estimation from statistical correlation between reaction rate, Oxygen concentration and temperature. The order of temperatures (from top) mimics the order in which they were performed during the experiment.

In the continuation, in order to better understand and study qualitatively the behavior of the carbon film towards oxidation and the dependence of the reactivity on the conversion, temperature and history of the sample, two pulsed-oxidation experiments were designed and performed through a series of step-response isothermal oxidations from the beginning to the full conversion of the carbon load on the sensor.

4.2.2 Carbon film qualitative investigations with Oxygen Sweep

In the study of the Carbon film oxidation there is a number of system components that need to be considered when working with the oxidation reaction. In the course of the events during an experiment, first comes the pre-treatment of the samples, which itself could be divided mainly into two parts. First comes the thermal treatment and second comes the oxygen exposure treatment. In the thermal part, it could be an isothermal treatment or a temperature programmed one, which could have its own implications on the subsequent kinetics depending on the nature of the carbonaceous matter under question. During this stage mostly the microstructural modifications of the system occur and lead to physical and chemical property changes before the actual oxidation experiment (as discussed above and elsewhere (3), (8)). This step can be advantageous

in terms of removing mentioned variants from carbonaceous matter e.g. dissociation of adsorbed species and reforming into stabilized structures as a result of heat treatment with the aim of rendering the least deviant conditions. Furthermore, introducing a series of O_2 pulses prior to main oxidation will remove highly reactive surface compounds adsorbed and possibly opens up new or clogged microstructure pathways as it pushes the reaction front for better diffusion of O_2 into the bulk of material. In order to test the validity and relevance of the mentioned considerations, and to see how the carbon film and specifically the reaction rate behaves as the oxidation front proceeds, the following experiments were designed and performed.

Experiment 1

Pre-treatment: The experiment began with a pre-treatment of the sample by a TPD step to a target temperature of 600°C with $10^\circ\text{C}/\text{min}$ ramp. This was followed by annealing at 600°C for 10 minutes. Also, in order to remove the adsorbed highly reactive surface compounds [7, 28], few short pulses of oxygen (10, 30, 10, 30 sec at 435°C and 3 vol.% of Oxygen) were included in the pre-treatment of the sample which is equivalent to oxidation of roughly few percent of the overall sample.

Oxidation: Afterwards a sweep of Oxygen exposures consisting of 3, 6, 10, 13, 16, 20 and 25 vol.% during 30 sec each and separated with 2 minutes of exposure to inert gas was carried out repeatedly at 375° and 400°C temperatures in an alternating fashion. Also a temperature of 435°C was placed between the 3rd and 4th sweep particularly for the purpose to assess temperature influence. The oxidation results and temperature sequences are shown in figure 25. The experiment mainly targeted the observations at the beginning, in the middle and toward the full conversion regarding qualitatively how reaction rate is influenced by conversion and temperature.

Bearing in mind that the $\text{ext}@800\text{nm}$ signal value is indicative of the amount of carbon left on the sample and the slope of its temporal evolution is a reaction rate representative, the immediate observation is that during O_2 exposure all the rates are almost linear and increase with increasing O_2 concentration during each sweep. Also by looking at the sequence of sweeps as the conversion proceeds the overall reaction rate and thus carbon consumption is increased when same reaction condition are repeated as three pairs of sweep are compared in the figure 26. In this figure the green-colored pair of sweeps was firstly done. Then a single sweep at 435°C was done (shown in figure 27) which was followed by blue pairs of sweep and finally the red pair.

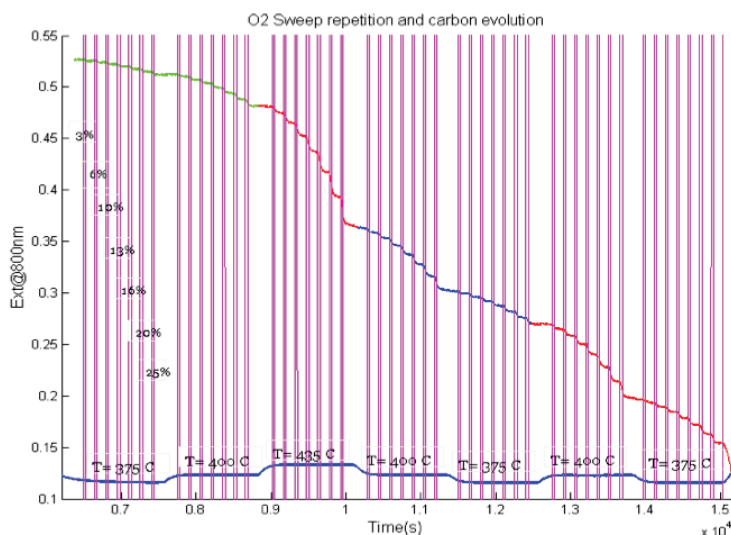


Figure 25 - Oxygen sweep experiment over one carbon film sample including reaction conditions and

resulting extinction signal. Purple bars are oxygen intervals and blue plateau at the bottom is the temperature during the experiment.

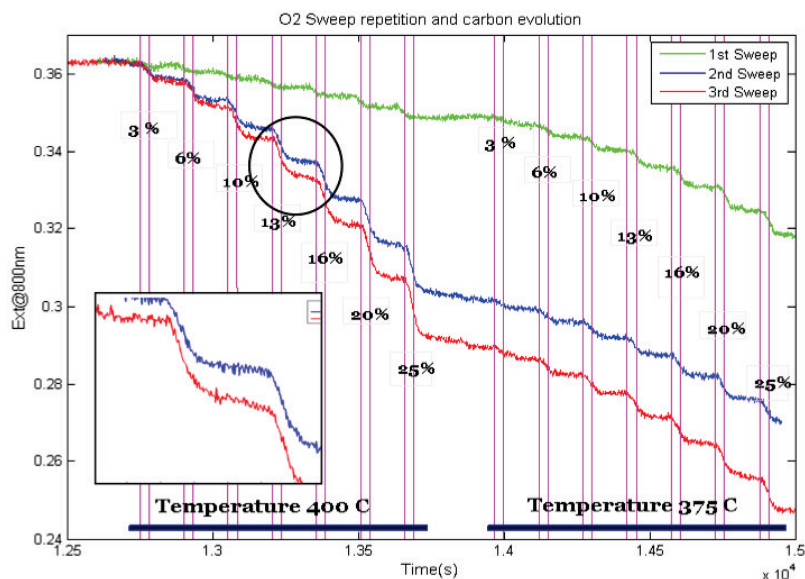


Figure 26 - Complete set of sweeps sorted by temperature and labeled in order of occurrence. As can be seen, sweeps two and three are closer to each other compared to first sweep due to the presence of an increased temperature step between sweep one and two. This clearly indicated the importance and influence of the sample history on subsequent oxidation.

This can be explained in line with the fact that as the oxidation proceeds the conversion of reactive and more accessible carbon promotes higher rates.

If the result of the sweeps are sorted based on the temperature and labeled in the order they have been performed, it can be easily seen that similar temperatures conclude nearly same rate and carbon conversion in each sweep as is presented in the figure 27. Also for higher temperature of 400° the rates are higher than for 375° C. For cases of sweep 4 and 6, as are evident the rates and total carbon consumption vary considerably from sweep 1 though performed at the same temperature. The difference can be ascribed to the effects of sweep 3 done at 435° C (indicated in figure 27), which has induced sudden increases in the reactivity and thus carbon consumption. This could be suggesting that sample history (temperature and possibly O_2 concentration) is probably influencing subsequent oxidations. From another point of view, the rates of sweeps 5 and 7 are not so different than sweep 2 which suggests that undertaking 435° C sweep, hasnt influenced the rates at sweeps 5 and 7.

So the first sweep difference with later isotherms might be due to the presence of oxidation occluding surface compounds still present on the surface (despite the preceding TPD step) and yet to be opened micro/nano structures after pre-treatment which later seems to be removed by a sweep at 435° C. Here to test this hypothesis, one either should perform another sweep at 435 C for comparison or perform an elevated temperature step without O_2 and the again run a sweep to just check the temperature effect.

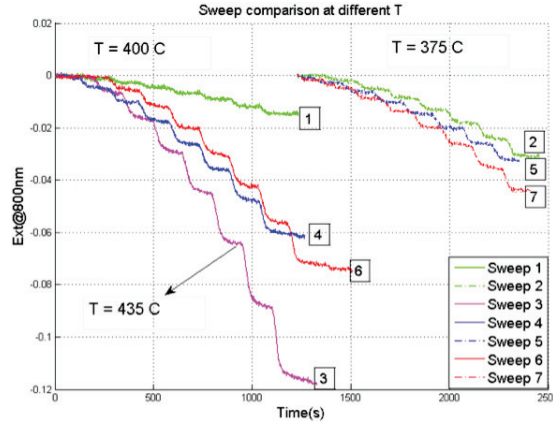


Figure 27 - Complete set of sweeps sorted by temperature and labeled in order of occurrence. The sweeps 2, 5 and 7 are closely following each other while all of them have been performed after a identical sweep at 400 C. The sweeps 4 is noticeably different

Experiment2

In the second experiment, as is illustrated in the figure 28 the default temperature of the experiment was chosen 410 C to maintain a low reaction rate and oxygen concentration of 10 vol.% was used. The oxidation was preceded with a TPD step from 21-600° C at 10° C/min and brought to 410° afterwards. Each 5 identical oxidation pulses of 30 s separated with 2 minutes in inert gas only were grouped in 1 block (or sweep) for averaging and ease of comparison and 12 such blocks were repeated. Also each block was separated from the next one by 4 min of inert Ar atmosphere. As can be seen, during the course of experiment, two temperature steps were introduced: one with oxidation and during block 5, and one without oxygen between block 8 and 9 for the same duration of a block, to study the effect of temperature on the reactivity.

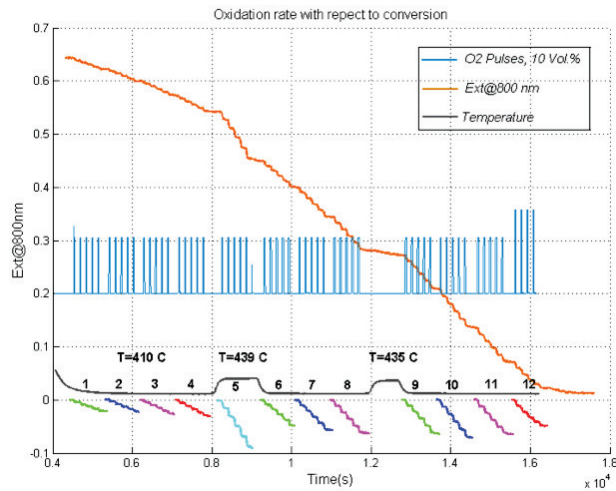


Figure 28 - Pulsed oxidation study of the 30 nm thick carbon film with corresponding extinction signal and oxidation conditions. Extinction signal during each block is also plotted at the bottom of the graph to show the relative drop of the signal i. e. reactivity.

Results of the experiment are investigated in the figure 29 where different blocks are compared to each other. As the duration and exposure of the oxygen within each block is the same for all blocks the converted carbon during each block is corresponding to the reaction rate of the oxidation in that interval. As can be seen, for the first 4 blocks with similar oxidation conditions the reactivity is increasing but only slightly from block 1 to block 4.

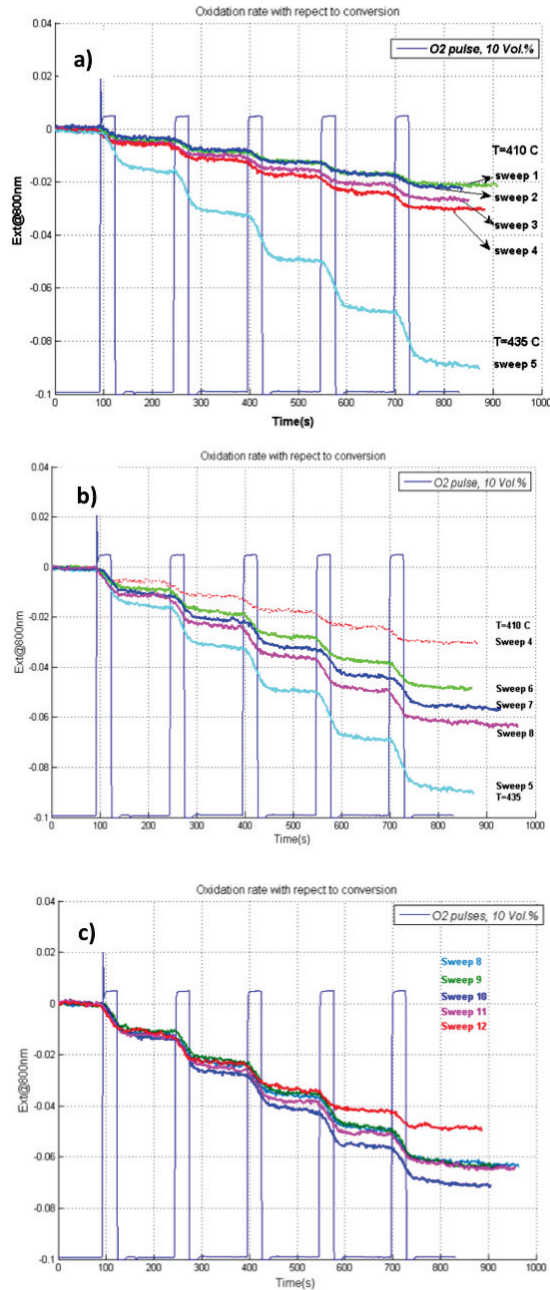


Figure 29-Isothermal pulsed oxidation and corresponding extinction signal for 12 consecutive group of pulses. Each pulse is 30 sec and separated from next pulse by 2 minutes to minimized self-heating effect. Extinction signal for the first 5 block of pulses in top panel, block 4-8 in middle panel and last five blocks in lower panel are depicted.

During the block 5, as the temperature is raised to 439° C a significant reaction rate increase is observed in figure 29 (a). Considering figure 29 (b) during the blocks 6, 7 and 8 as the temperature is brought back to 410° C, the reaction rates undertakes a decrease compared to the block 5, yet it is higher compared to the block 4 and gradually is increasing from 6 to 8. It is worth to note that carbon consumption difference of block 4 and 6 is higher than the difference between sequential isothermal blocks. This is indicative of the fact that the reactivity has increased as a result of higher temperature oxidation and this might suggest that sample history could be important in determining the reaction rate. This can be further supported with observation during second temperature step without oxygen introduction. As is shown in the figure 29 (c) the carbon consumption difference of block 8 and 9 where between there is a temperature step with duration of a block, does not seem to change at all. This is clearly seen with the complete overlap of the extinction signals during block 8 and 9. In the continuation of the experiment the rates start to decrease from block 10 to 12 as the carbon balance is diminishing.

An overall comparison of all the rates over the entire conversion is depicted in the figure 30. The un-normalized rate obtained during the experiment, normalized rate by shrinking core model and for the case of carbon reaction order of 1 are plotted as function of conversion. Results are in a consistent behavior as to those of Printex-U published elsewhere (2).

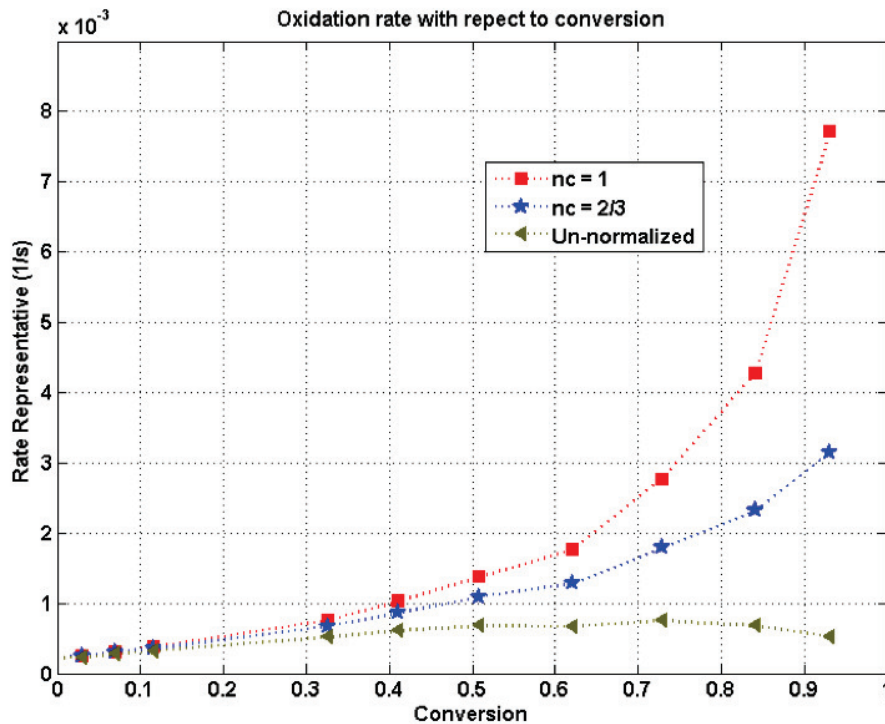


Figure 30 - Oxidation rate of the carbon film with respect to conversion degree. For each block a point representing the rate calculated as carbon consumption over oxygen exposure time is drawn for an un-normalized rate. Normalized reaction rate ($r_{norm} = r/f(x)$) with $f = m_{init}(1 - X)^{n_c}$ for two cases of $n_c = 1$ and $2/3$ are plotted.

References

1. Larsson, Elin. Nanoplasmonic Sensing- From Biology to Catalysis. s.l. : CHALMERS, 2009.
2. Experimental method for kinetic studies of gas-solid reactions: Oxidation of the carbonaceous matter. Carolin Wang-Hansen, Carl J. Kamp, Magnus Skoglundh, Bengt Andersson, Per-Anders Carlsson. 2011, J. Phys. Chem. C , pp. 1609816108.
3. Temperature Dependence on Structural, Tribological, and Electrical Properties of Sputtered Conductive Carbon Thin Films. Yong Seob Park, Byungyou Hong, Sang-Jin Cho, Jin-Hyo Boo. s.l. : Bull. Korean Chem. Soc., 2011, Vol. 32, p. 3939.
4. Development and validation of a model for the chemical kinetics of graphite oxidation. Mohamed S. El-Genk, Jean-Michel P. Tournier. 411 , 2011 , Nuclear Materials, pp. 193207.
5. Zacharia, Renju. Desorption of gases from graphitic and porous carbon surfaces, PhD Dissertation. s.l. : Freien Universitt Berlin, 2004.
6. The oxidation of soot: a review of experiments, mechanisms and models. Stanmore, B.R., J.F. Brilhac, P. Gilot,. s.l. : Carbon, 2001, Vol. 39, pp. 22472268 .
7. Investigation of the oxidation behavior of diesel particulate matter. Aleksey Yezerets, Neal W. Currier, Heather A. Eadler, Arvind Suresh, Paula F. Madden, Mark A. Branigin. 88 , 2003, Catalysis Today, pp. 1725.
8. Differential kinetic analysis of diesel particulate matter (soot) oxidation by oxygen using a stepresponse technique. Aleksey Yezerets, Neal W. Currier, Do Heui Kim, Heather A. Eadler, William S. Epling, Charles H.F. Peden. 2005, Applied Catalysis B: Environmental , Vol. 61, pp. 120-129.

Chapter 5

Concluding Remarks

This project aimed at investigating the possibility to apply the Indirect Nanoplasmonic Sensing platform (Insplosion AB, Gteborg, Sweden) as a new tool for in situ carbonaceous matter oxidation studies. For thermally evaporated carbon films of 5 and 10 nm thickness as the sample material, the platform showed a good sensitivity and could reveal some of the properties of the oxidation process, such as oxidation onset, carbon removal rate, and dependencies of the latter on temperature and oxidant concentration.

For an alternative soot representative material, i.e. Printex U, it was found that deposition of the material on the sensor chips with a good coverage resulting in enough sensitivity is not straightforward and needs more effort than the methods tested in this thesis. Hence, throughout the thesis only thermally evaporated carbon was used as sample material for kinetic studies. Using the Arrhenius formalism it was possible to estimate their activation energy of the reaction for a set of isothermal oxidation data. The obtained values are very close to the range of previously published results. For the latter data set (obtained in 21 vol% O_2), significantly lower activation energy was obtained.

In general the series of progressive isothermal step response experiments showed expected trends of the reaction rate. However, detailed kinetic evaluation of the measured rates resulting in a full range of kinetic parameters was not realized due to problems mainly associated with irreproducibility between experiments. Irreproducibility was found to be originating mainly from carbon film properties and direct influence on the oxidation process via uncontrolled self-heating of the reaction, microstructural and reactivity variations between different samples and changes of the carbon surface itself during heat treatment and progressive oxidation.

Furthermore, the INPS signals, i.e. the plasmonic peak shift and extinction signals used here were found to be a function of temperature of oxidation. Particularly for higher temperatures, the extinction signal initial increased for constant carbon films thickness (resembling a larger total carbon load), which in turn could result in observing higher rates during gasification, than the actual mere temperature-induced rate. This effect though small, is present and thus propagated modifications in the data could shadow the direct comparison of the oxidation profiles done at different temperatures. This, consequently, could alter the results when it comes to a kinetic analysis.

It is also important to note that, due to the nature of the colloidal lithography used in the fabrication of INPS chips (i.e. the fact that it is a serial fabrication yielding chips not perfectly identical), different sensors may exhibit slightly different sensitivity towards reaction in general. The latter despite being present, does not seem to be an issue for the extinction signal at 800 nm (which is almost independent of the plasmonic resonance and is referenced by blank measurement) used in the kinetic analysis but should be considered when using the plasmonic peak signal.

In a second set of redesigned experiments, differential oxidation was used as a strategy to overcome some

of the problems associated with irreproducibility of progressive oxidations. This approach allowed for gaining more consistent rate dependence according to the reactive condition and also resulted in extracting the reaction order of oxygen within the range of reported values. The found reaction order was furthermore revealed to be conversion dependent. Moreover, an analysis of the experimental data using a shrinking core model yielded a conversion dependence of the rate, which was comparable to those published in the literature.

Finally, also using differential oxidation experiments, the qualitative properties of the used carbon films were investigated. The dependence of the reaction rate on the thermal history of the sample was analyzed. We found that under the same oxidation conditions, based on the previous oxidation conditions, different oxidation rates will occur. For example, when an oxidation step at a higher temperature is placed between two isothermal oxidations at identical lower temperature, different rates will be observed. Interestingly, however, the history does not alter the oxidation rates if an intermediate temperature raise is performed in inert rather than oxidizing atmosphere.

Chapter 6

Outlook

Throughout this project we primarily aimed at exploring INPS ability to follow the kinetics of the oxidation reaction of carbonaceous matter. As for investigating any new methodology the primary focus was placed on (i) using a simple carbon model system (instead of real soot) and (ii) using well-known kinetic models relying on conventional global rate expressions and the Arrhenius formalism to interpret the rates into the kinetic parameters.

For the case of a complete set of isothermal oxidation experiments, due to carbon reactivity related issues and other mentioned factors causing irreproducibility between nominally identical experiments, however, utilization of a global kinetic model was not possible. Therefore it would be very essential to overcome this problem by developing a new procedure to control and minimize variants among different samples such as carbon film packing, surface termination, defect concentrations and a more controlled reaction environment to minimize local temperature increase stemming from the exothermic oxidation reaction (and locally altering the reaction rate), which all can interfere with the reaction kinetics studies. These procedures could include pretreatment of the samples before oxidation by thermal and oxidant exposure steps and active heat management to efficiently get rid of the reaction heat.

Another important issue is the dependence of carbon reactivity on thermal history, which seems necessary to be fully examined by a series of intermittent temperature cycles. Confirmation of restructuring/ordering of graphitic carbon could additionally be studied by incorporating other techniques such as in-situ Raman spectroscopy, electron microscopy and BET measurements.

As for deposition of the carbonaceous matter on the INPS chips, it seems that more effort is necessary for the development of a more straightforward and easier way of deposition (currently PVD of films in clean room, costly, time consuming and prone to induce variations in carbon films), comparable to the deposition of reference carbon, e. g. Printex U, on monoliths done by mechanical shaking. Also for the ultimate purpose of soot oxidation studies, which is of high technical importance, deposition of soot with efficient and better attachment should be realized. This might be done by tailoring spacer layer surface chemistry of the INPS chip and by establishing deposition methods optimized for the soot physical and chemical properties such as hydrophobicity and static charge.

Moreover, to fully utilize the power of INPS, other parameters extractable from absorption spectra such as plasmonic peak and more could be considered. Before that, owing to the fact that the plasmonic peak is not in linear relationship (as opposed to extinction signal) with measuring signal (carbon load) and is a function of other parameters such as distance of reaction from surface as a result of exponential dependence of enhanced LSP field, it is not possible to use this signal directly for a kinetic analysis. A possibility then is to determine other contributing parameters in the signal theoretically or/and empirically and finally decouple such effect from the measured signal. This will enable more straightforward signal interpretation specifically if INPS is to be used for kinetic studies.

Considering the fact that the extinction signal used in this study as the main signal for the kinetic analysis, is representative of the carbon load left on the sample, and the fact that signal slope is rate representative, as a suggestion, it can be more helpful for kinetic studies to develop the Insploer software to directly calculate for the rate of the signal changes. This can bring improvements in the accuracy of the kinetic calculations, which require rate data rather than direct signal, which is recorded in todays version of the software.

Acknowledgement

The time of my thesis project has been a process for me to learn, create, develop, be challenged, accomplish and grow in certain aspects. All these, of course, has been promoted and delicately shaped as it is now with presence of people along the way during the journey of this project and I would like to take this opportunity to say few words about them.

I would like to begin with saying thank you to **Elin Larsson**, my caring lab supervisor for all her help with experiments, being present all the time for my questions and discussions and most importantly, inspiring me to understand better about the nature of research and how to do deal with unexpected situations. Hope you are enjoying your time with your new born son and Im very much thankful to you.

I would also like to express my sincere gratitudes to **Christoph Langhammer**, my expert supervisor in nanoplasmonic and examiner for all guidance and fruitful discussions during project and specially being always so accurate and precise, very encouraging and giving me the opportunity to explore my way around the challenges that project offered. Many thanks to you indeed and wish you luck with all your ongoing projects.

Afterwards, I am going to thank you **Per-Anders Carlsson**, as my carbon-expert supervisor for all the help and discussions we had. Our discussions here and there were my clues to explore more into the details and project pores to finally nail down some of the tackles we were exposed. Thank you very much.

Thank you **Pooya** for making the INPS sensors for me and for all help in the lab, also for being so nice colleague and friend, for lots of fun and interesting continuous discussions from plasmonics, to cosmos, consciousness and even more to our Chit-Chang theory .

Im very much thankful to **Svetlana**, for always being helpful and so nice to make my samples in clean room.

Furthermore Im thankful to **Soran**, such a friendly and open colleagues and a former colleague **Carolin** for their help and answering my questions.

I would also like to thank **Dr. Aleksey Yezerets**, for being extremely nice and spending your precious time to try to come up with advices associated with my project, even on phone and from transatlantic while being swamp at work.

This is also my words to my very awesome friends that always have made me happy and joyful, especially during the intense times of the project, bringing good mood and energy, specifically thank you **Sasha, Ali, Bayat** and **Mooli**.

This study has been performed at the Competence Centre for Catalysis, which is financially supported by Chalmers University of Technology, the Swedish Energy Agency and the member companies: AB Volvo, Volvo Car Corporation, Scania CV AB, Haldor Topse A/S and ECAPS AB.

Also I would like to thank all people at KCK and Chemical Physics division for they contributed to such a nice and collaborative environment that I worked in and enjoyed my time.

The last but not least, to **my all love family**: Im always thankful to you for your great support and compassion. You have shown me what a big heart looks like and have given me a back pack for an enjoyable life, I love you always.

Appendix A: Printex U model Soot deposition and Oxidation Studies with INPS

This section describes the results from the first part of the project, i.e. deposition and oxidation of Printex U on the INPS sensor chips. This includes a number of methods tested during this project, which I will describe in this section, and a summary of the results.

A.1 Soot Deposition

A.1.1 Mechanical shaking method

Mechanical shaking of soot with INPS sensor chips in plastic containers was selected as the first deposition procedure. As the coverage of soot on the sensor chip can be connected to the amount of the soot being used and the shaking time a total of 20 combinations of shaking time (10, 20, 40, 60 & 80 sec) and soot amount (0.005, 0.01, 0.025 and 0.05 gr) were selected and tested. Each combination was also repeated three times and the average result was used (60 experiments in total). The calibration was obtained using a spectrophotometer (Cary 5000) and taking three absorption spectra for each single deposition. One before shaking of the sample as blank reference, second after deposition of soot and a third one after removal of the soot from the sensor. The removal of soot was done by means of sonication of sensor chip in the Aceton for about a minute, rinsing with ethanol and distilled water and blow dry with Nitrogen. During the deposition step, the backside of the sensor chips were covered with a clean room class adhesive tape in order to avoid deposition of the soot on the back side. The absorption peak shifts in each of the experiments were correlated with to the soot weight and also the shaking time. Results are sorted versus time and the initial soot weight and are shown in the figure 31. The same data also sorted versus time of the shaking are presented in figure 32. It was attempted to fit a line to each of these data sets in search of any correlation. As it can be seen from the slope of the fitted lines, barely any correlation seems to exist. This means that the adhesion of the soot particles to the silica layer is not connected to the time of shaking or initial soot weight but instead a random behavior. In order to test if the electrostatic charge of the soot originates from the plastic containers used for shaking, glass containers were used instead, with aluminum foil cap to reduce the soot electrostatic charge. This alternative procedure, however, didnt improve the adhesion behavior of Printex U.

A.1.2 Spin coating method

In another effort the plasmonic peak shifts and extinction changes upon spin coating (10000 rpm) were measured for soot dispersed in ethanol in five different concentrations of 0.005, 0.01, 0.02, 0.04 and 0.08 gr per 10ml. All suspensions were sonicated for at least 3 minutes and just before the spin coating to reach finest dispersion. Soot aggregates showed to be dispersable in the acetone while a large number of big chunks of aggregates were observed in the ethanol with sedimentation after few tens of minutes.

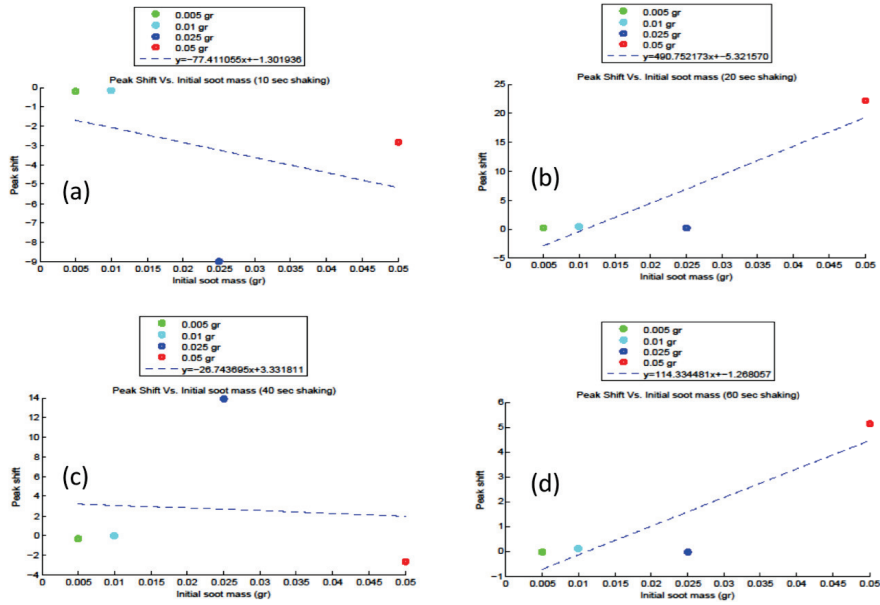


Figure 31 - Shaking results versus PrintexU initial mass. In each graph peak shifts versus soot weight for four different soot masses are plotted. Each point is the average of the three peak shifts measured. Also each graph represents results from a certain shaking time including 10 sec (a), 20 sec (b), 40 sec (c) and 60 sec (d).

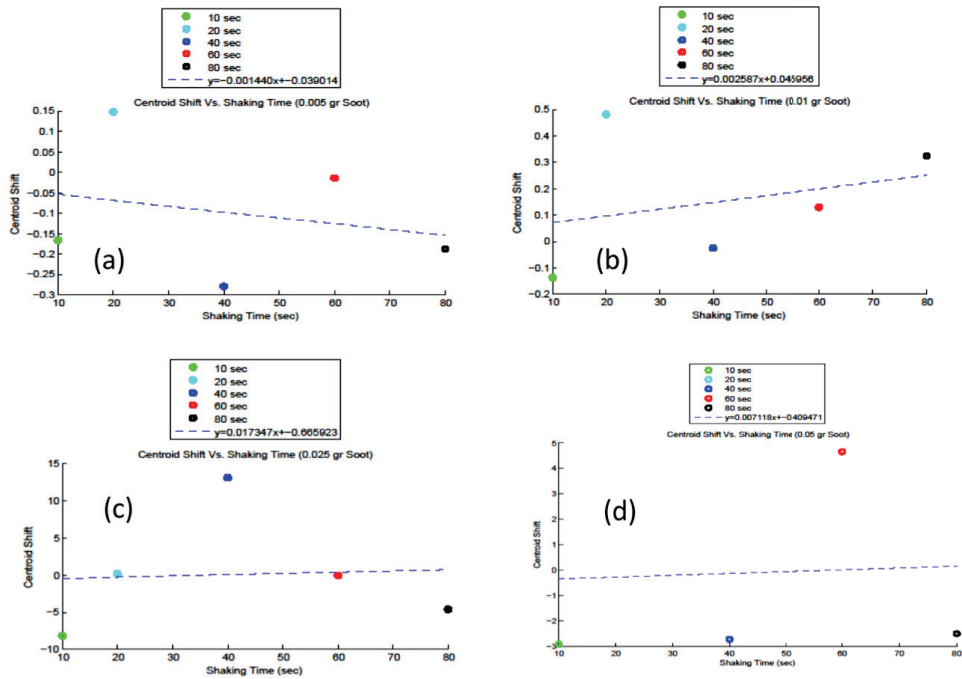


Figure 32 - Shaking result versus shaking time. In each graph peak shifts versus shaking time for five different shaking times are plotted. Each point is the average of the three peak shifts measured. Also each graph represents results from a certain initial soot weight (a) 0.005 gr, (b) 0.01 gr, (c) 0.025 gr, (d) 0.05 gr.

Solvents, though not favored for the fact that they could alter the soot behavior during the oxidation, were tested to identify a methodology capable of forming a high (for stronger signal) yet thin (allowing for particles to remain in the sensing volume) coverage of the soot on the INPS sensor chips. For each concentration three sensors were used to produce three data points. The results are shown in figure 33 (a) & (b):

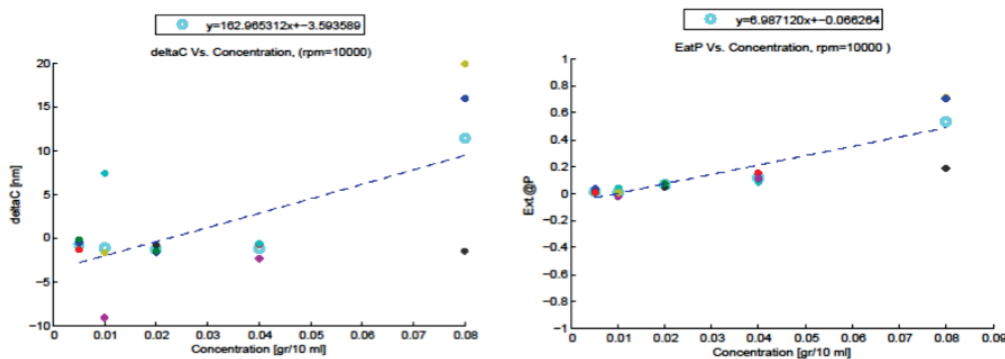


Figure 33 - Result of the Printex U deposited by spin coating from Acetone and correlation of absorption spectra with suspension concentrations. Centroid shift vs. concentration (a) and extinction vs. concentration (b) Light blue circles are averages of three data points. The linear fit and all data points are shown.

The extinction signal exhibited a more clear trend as an incline with concentration increase compared to centroid shift. Nevertheless no truly significant connection between the concentration increments and increased extinction is observed for four used concentrations. For qualitative comparison of the different deposition methods bright field optical images of samples prepared by shaking and spin coating are presented in the figure 34. Soot aggregates seem to have a large z-direction height so that most of the soot is not in direct contact with the surface and mostly outside of the sensing volume volume of the sensor (the sensing volume extends a few tens of nm from the sensor surface). This is found by changing the focal plane of the objective by a tiny fraction, which is much larger compared to the sensing depth, while scanning different z-stacks of one typical soot agglomerate.

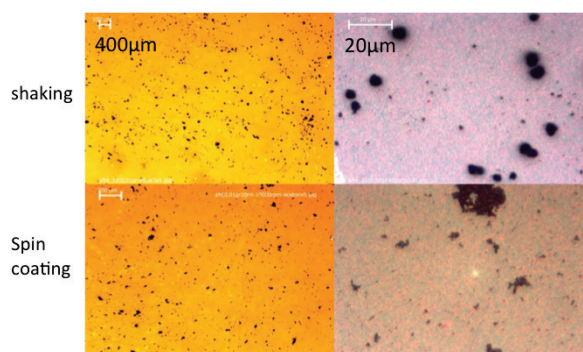


Figure 34 - Mechanical Shaking (up) and solution spin coating (down) samples optical images show not much difference between two methods used. Also It was found that soot agglomerates are more flat in the spin coating method, since a different z-stacking of a certain soot agglomerate in shaken samples could come to focal plane with zooming in and out while imaging.

A.1.3 Thick layer of soot

In an attempt to reach a thin (transparent) uniform layer of soot on the sensor chip, a highly concentrated of soot suspension in EtOH (0.8 gr/10ml) was dropped on the sensor and left to dry in room ambient temperature. As a result a thin (sub-millimeter yet not transparent), highly smooth and condensed layer of soot is formed on the sensor. The idea was to reach a very thin layer after enough oxidation time and then use the data very close to the end of the experiment where it was imagined to be an ideal few-tens-of-nanometer layer of soot. A number of oxidation experiments were performed but the data showed a very noisy behavior. To further investigate this observation, in one oxidation run the experiment was interrupted in the middle and the sensor was taken out for qualitative check. As shown in Figure 35 the soot layer was found to consist of fragile large flakes partly detached from the sensor surface. This is partially due to the different oxidation rates of soot from different directions and due to shrinkage and different thermal expansions of soot and sensor upon heating.

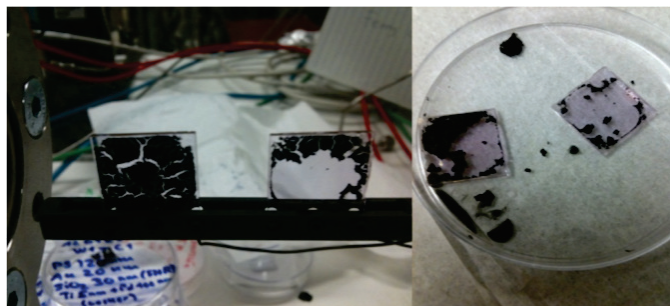


Figure 35- Thick layer of soot in the middle of oxidation.

A.1.4 Airbrush spray

As another attempt, an airbrush was used to spray a suspension of soot onto surface of the sensor. Suspension of soot in both acetone and ethanol were sprayed for roughly 2 seconds with the same spray power and results were checked with optical microscopy. After drying off the solvents, the optical microscopy images showed rather large soot aggregates on the sensor surface (similar to what is obtained by the shaking method), which above has been proven to be problematic for the signal to noise ratio and sensitivity.

A.1.5 SEM Images

To answer some of the ambiguities regarding the sporadic behavior of absorption spectra obtained for the same sensor with and without soot, SEM images of the samples produced by different procedures such as shaking, spin coating, spraying and air dried drops were acquired. SEM micrographs reveal that the obtained soot aggregates are of much larger size and thickness than the gold nanoparticles (110nm) of the INSP sensor. Moreover only a small fraction of the sensor surface is covered by soot. Hence, only a tiny fraction of the gold nanoparticles end up at a short enough distance from smaller spherules for the latter to (i) be inside the sensing volume and (ii) consequently give rise to a shift of the Plasmon frequency upon oxidation. As can be seen in Fig. 36 (a-d) the soot aggregate distribution on the surface is such that (particles of $\sim 200\text{-}20000\text{ nm}$) they either block a large area that light probably cant pass, and for other areas, where the light can pass, the distribution is very low and the fraction of the gold nanodisks that are influenced by spherules ($20\text{-}50\text{ nm}$) and particles ($0.1\text{-}1\ \mu\text{m}$) is so small that their effect on the plasmonic resonance is almost negligible compared to the integral average of gold particles which are being read off by the light beam.

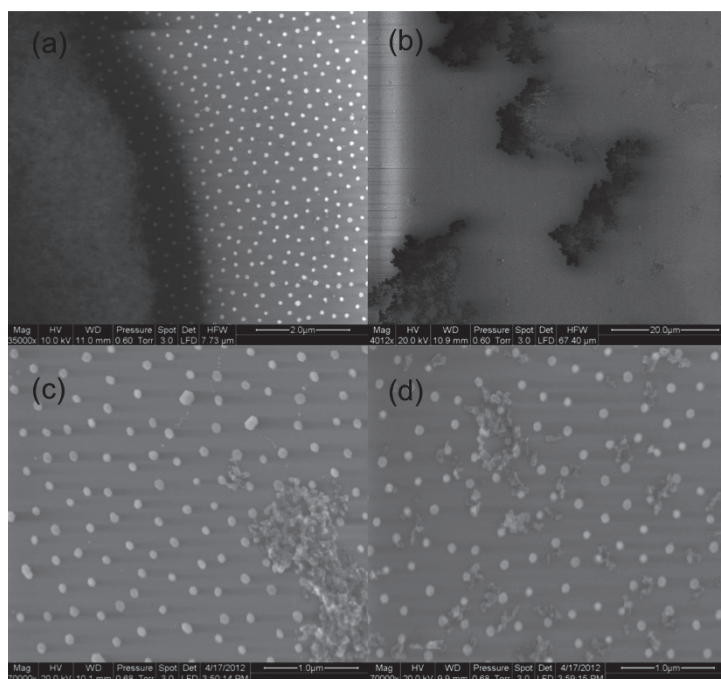


Figure 36 - SEM micrographs of Soot on gold nanoparticles deposited with different methods. Samples are prepared by dried drop (a), spraying of soot solution (b), spin coating (c) and shaking (d).

Furthermore it is observed that the case of shaking in general prevents the aggregation of soot and a homogenous soot distribution (including least number of aggregates and presence of particles down to few spherules) is achieved by the shaking method but in glass containers instead of plastic ones in excess of soot and shaking for about few minutes and finally strongly blowing the sensor surface with Nitrogen gas to remove larger aggregates where the smallest particles would yet attach firmly. A result of such a procedure is displayed in Figure 37. This method improves the deposition, and was used in the oxidation experiments. However, as will be shown in the next section, it still renders a very small plasmonic peak shift signal.

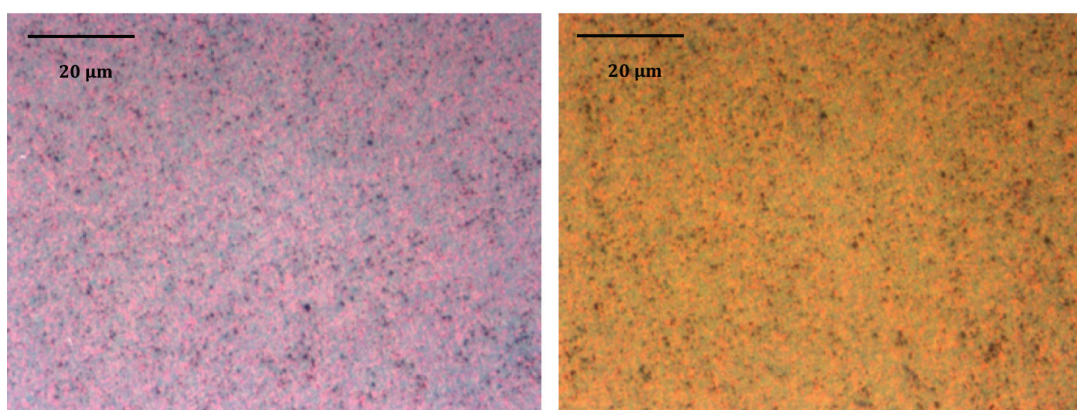


Figure 37 - Optical microscope image of two distinct sensors shaken with soot for 5 min and the blown strongly.

A.2 Step-Response Oxidation of Printex-U

A.2.1 Isothermal Oxidation

Oxidation experiments on samples prepared by the mentioned shaking method were performed for two sensors, both prepared alike, i.e. 5 min shaking in large amount of soot (1 gr). An oxygen concentration of 2%, a temperature of 550 C and a total 170 ml/min flow rate were chosen during a step-response experiment. In addition this experiment was repeated twice for a reproducibility check. The temperature was raised by a fast ramp (45 C/min) to the destination temperature and maintained for around 40 min in Ar before oxidation. The resulting centroid and peak signals of the two experiments No. 1 (left) and No. 2 (right) are depicted in the figure 38 and signals for both sensors in each experiment are plotted.

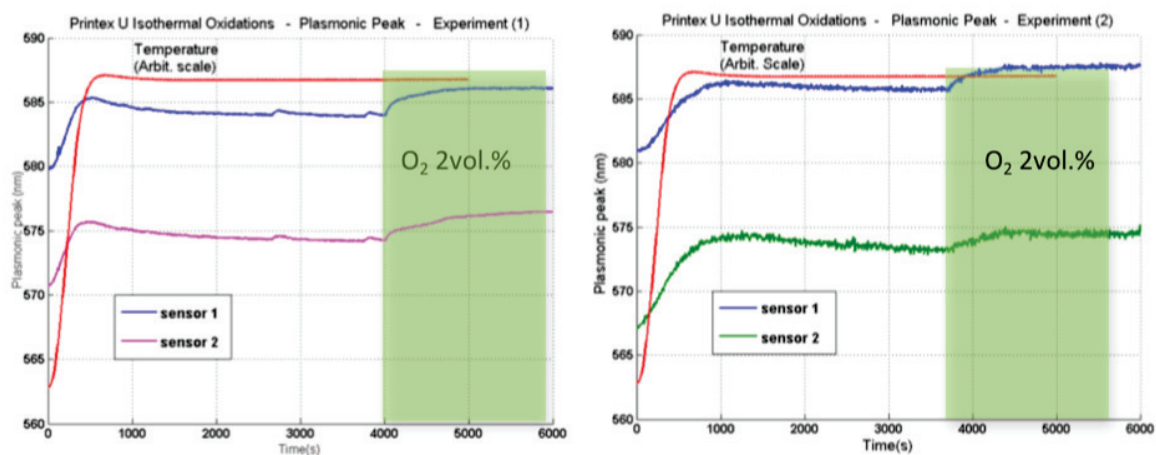


Figure 38 - Plasmonic peak for two similar oxidations experiments with same two sensors. Oxygen introduction is corresponding to the discontinuity point in the signals. The centroid and peak behavior in the first experiment (left) and second one (right) are observed as red shift between 2 to 3 nm.

A.2.2 Reproducibility of one sensor

In the following, plasmonic peak shifts of each of the sensors similarly treated as in the two mentioned experiments above are analyzed for reproducibility of one sensor. Figure 39, demonstrates the normalized behavior of each of the sensors in two similar oxidation experiment via plotting normalized plasmonic responses during the Printex U oxidation of each sensor. In the original values we observe a horizontal shift of 1.5 nm in the peak position from experiment one to experiment two, which is simply due to the fact that we are not measuring exactly on the same spot on the sensor during repeated experiments. Apart for these slightly different start values of the plasmonic peak position, the measured sensor response during oxidation of the soot is the same for sensor one (as very nicely illustrated in the normalized data in Figure 39), which indicates reasonable reproducibility. For the case of sensor two the results for two subsequent measurements deviate more, presumably due to different amounts of soot present on the surface and/or other reasons discussed above. One interesting observation, common to all experiments, is the presence of a kink in the oxidation curve at about 0.6-0.8 conversion.

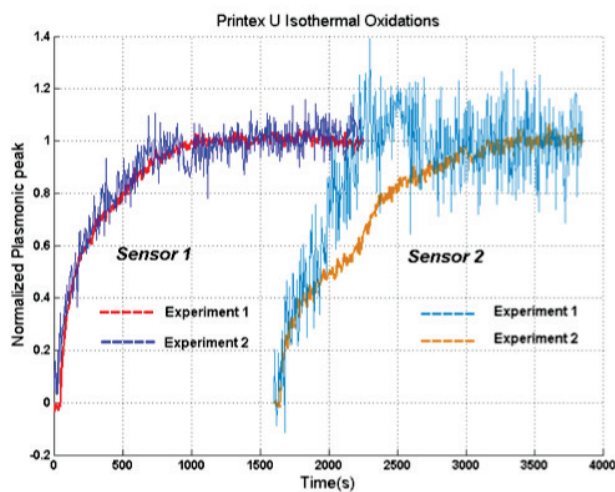


Figure 39 - Normalized plasmonic peak for each of the sensors plotted on top of each other for reproducibility control.

In the continuation several isothermal identical oxidations ($T=550\text{ C}$ and $2\text{ vol.}\% O_2$) were performed on different sensors, onto which Printex U was deposited with the described shaking method to check the reproducibility between different samples similarly prepared. The results are shown in the figure 40 and 41.

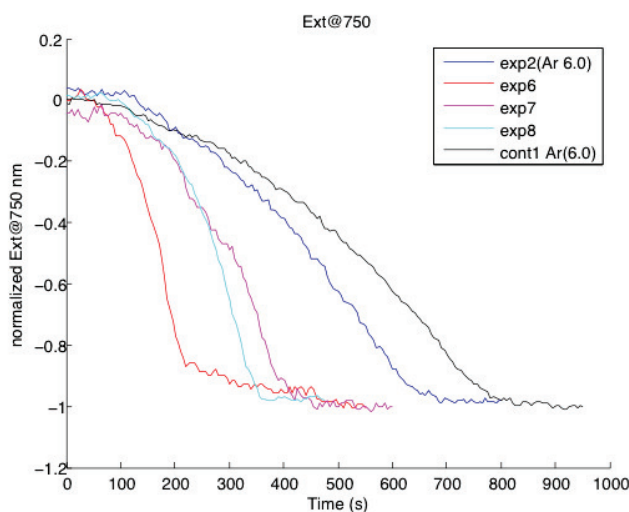


Figure 40 Normalized Extinction@750 nm during oxidation interval of several identical oxidations with Printex U.

As can be seen in the figures, the reproducibility is still a subject of discussion. Different sensors respond differently to the same reaction as a result of variations in their properties created during fabrication or, most likely also due to differences of the deposited amount and type of soot (spherules vs. aggregates which may have different reaction kinetics).

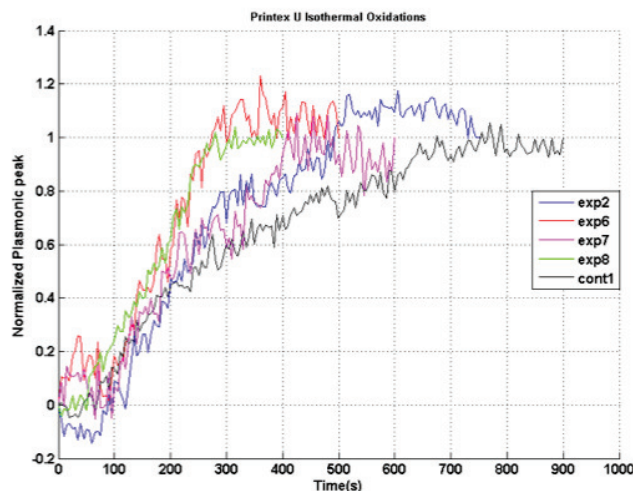


Figure 41-Normalized plasmonic peak for several similar oxidations of Printex U done at 550 C and 2 vol.% O₂.

One fact that is worthwhile to note is the red shift of the plasmonic peak position and centroid as a result of the oxidation process. From studies on LSPR sensors in bio- and chemosensing (1) it is known that a red shift occurs upon increasing refractive index on the surface, which normally means an adsorption or a binding process. However, here it is the gasification and *removal* of the synthetic soot from the surface (which has a higher refractive index than air), which is causing the shift. Hence the observed red shift is somewhat surprising. On the other hand, from the extinction intensity observation, a reduction in the signal is happening which clearly is indicator of surface species removal in the same experiment.

A.2.3 Signal compensated for the gas switching

Since the plasmonic peak in the INPS setup was found to be sensitive to switching between feed gases, another experiment was designed to deconvolute the effect of the gas switching and the soot oxidation on the peak position shift. For this purpose oxygen exposure of two sensors simultaneously in the reactor - one loaded with Printex U and the other blank - was carried out at 550 C and 170 ml/minute flow rate. Two prolonged O₂ exposures with inert atmosphere in between the exposures were used in a step response fashion. During the first oxidation, the loaded sensor signal corresponds to the sum of the soot and gas switching effects. The second oxidation, carried out after oxidizing the synthetic soot and remaining in Ar for few hours, the reveals only the gas switching influence on each of the sensors. The differences between the two signals will yield the true response from the soot oxidation. The blank sensor is used as a reference for such effect in parallel to the loaded sensor and should yield the same response in both oxidation steps. In figure 42 the peak position for both sensors are plotted and a summary of the result is presented in table 3. In the data shown in Figure 42 the plasmonic peak values from the onset of second oxidation step were subtracted from first O₂ exposure signal to exclude the gas switching effects and the resulting signal difference is plotted in red in the figure 42. Note that the signal for the two sensor are identical during the second oxidation step, once the soot has been removed from the blue sensor during the first step.

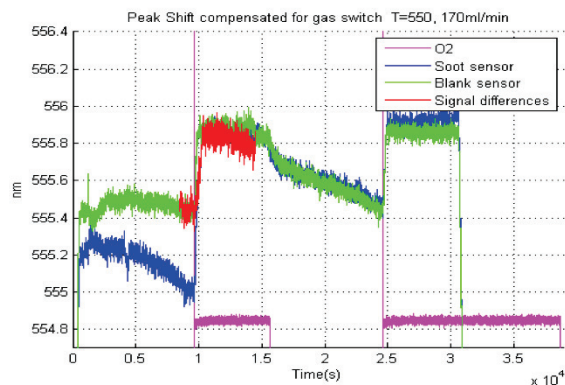
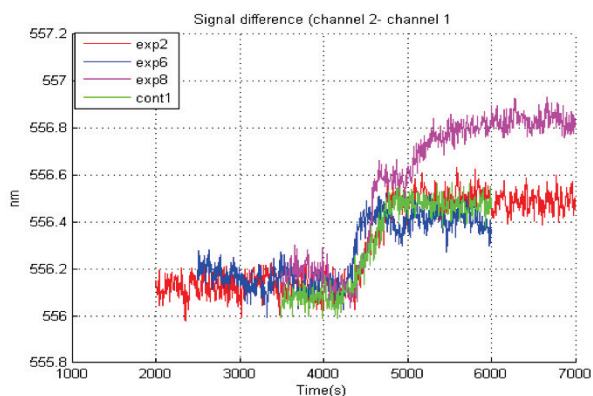


Figure 42 - Plasmonic peak position values for two sensors on loaded with soot and one blank. The red curve represents the signal difference between two intermittent O_2 exposures for the loaded sample and shows a 0.4 nm red shift.

Sensor	ΔP in first O_2 exposure	ΔP in second O_2 exposure
With Printex U	0.9	0.5
Blank	0.5	0.5

Table 3 - Summary of the results from both sensors and plasmonic peak shifts.

For the same experiment ($T=550$ C and 170 ml/min flow rate) peak positions compensated for gas switching are plotted for four different sets of data in figure 43. Its interesting to note that the shifts are approximately equal and around 0.4 nm.



43- The signal from a blank sensor is subtracted from the signal obtained for a sensor with soot (two different sensors). Curves are vertically and horizontally shifted to be shown in the same region.

References

1. Larsson, Elin. Nanoplasmonic Sensing- From Biology to Catalysis. s.l. : CHALMERS, 2009.